

**Fig. 1.** Simplified sketch showing the main features of a metamorphic core complex, modified after Brun & van den Driessche (1994).

*et al.* 2004b; Endrun *et al.* 2008). Pervasive flowing of the lower crust, thought to be possible if the rocks are of sufficiently low viscosity, is usually viewed as the most likely mechanism accounting for the flatness of the Moho in such regions (e.g. Block & Royden 1990; Buck 1991; Wernicke 1992; Brun & van den Driessche 1994; McKenzie *et al.* 2000).

The mechanics of MCC development and associated process of lower crustal flow have been addressed in several analytical, numerical and analogue modelling studies so far (Block & Royden 1990; Buck 1991; Wdowinski & Axen 1992; Brun *et al.* 1994; Rosenbaum *et al.* 2005; Wijns *et al.* 2005; Tirel *et al.* 2006; Gessner *et al.* 2007). In these studies, the modelling setup is generally concerned with the crust only; the way extension is accommodated in the underlying mantle is not addressed. More recently, Tirel *et al.* (2004a, 2008) have carried out numerical experiments with a setup encompassing the subcrustal mantle. Among these experiments, those involving a very high initial geothermal gradient are characterized by a greater complexity in the development of detachment zones, with commonly several synthetic and antithetic shear zones being formed in sequence during the growth of a single large MCC. In other words, these experiments tend to display strain delocalization during extension. However, for the purpose of a parametric analysis, this study needed to share the same shortcoming as previous studies did: the initial setup included a local heterogeneity forcing deformation to localize at a given site, enabling only one MCC to develop.

In the present study, we have performed new lithospheric-scale experiments in which deformation is not *a priori* localized in a specific place (the initial model is perfectly homogeneous laterally, and the grid is randomly distributed), in order to examine whether multiple MCCs could develop during extension, at which conditions, and how. A relatively wide range of initial conditions produced two-dimensional numerical configurations with either a single MCC or several far-distant MCCs aligned in the section parallel to extension. Extrapolated to a three-dimensional setting, the latter case suggests that distinct subparallel chains of MCCs could be a common situation in nature, provided the appropriate conditions are maintained over a region wide enough. In contrast, only a narrow range of conditions led to the development of closely spaced MCCs. In this case, because of the close spacing, the MCCs interfere with one another (the domes are partly superimposed or/and share a shear zone in common) and develop in sequence. The fact that this configuration is obtained for only a narrow range of conditions suggests that it should be rare in nature. Conversely, if it is observed in a natural setting, some insight may be gained from the experiments about the mechanics of extension and the physical properties of the lithosphere at the onset of the extensional event in the region.

The case of several MCCs aligned in a section parallel to the direction of extension is not uncommon worldwide. Examples may be found in the North American Cordillera (Coney 1980; Wust 1986), especially in the southernmost Basin and

117 Range (Davis 1980) and around the border between  
 118 USA and Canada (Parrish *et al.* 1988;  
 119 Vanderhaeghe & Teyssier 2001), also possibly at  
 120 the latitude of the Snake Range and in the central  
 121 Basin and Range (Wernicke 1992). The French  
 122 Massif Central provides another example (Burg  
 123 *et al.* 1994; Vanderhaeghe & Teyssier 2001). In  
 124 the Mediterranean area, this situation is encountered  
 125 in the northern Tyrrhenian domain (Jolivet *et al.*  
 126 1998) and, within the Aegean domain, in the  
 127 Cyclades archipelago (Lister *et al.* 1984; Gautier &  
 128 Brun 1994a, b; Jolivet *et al.* 2004) and in the nearby  
 129 Menderes Massif of western Turkey (Bozkurt 2001;  
 130 Gessner *et al.* 2001).

131 The Cyclades archipelago constitutes a particu-  
 132 larly interesting example because it has been  
 133 argued earlier that the islands form closely spaced  
 134 chains of MCCs that interfere with one another  
 135 (Gautier & Brun 1994a, b). In the following, we  
 136 first describe our numerical experiments, then  
 137 review the structural and metamorphic evolution of  
 138 the Cyclades. We subsequently compare the numeri-  
 139 cal results with the Cyclades. The comparison  
 140 concerns the final depth of the Moho, the geometry  
 141 of the MCCs, their kinematic pattern and the timing  
 142 of exhumation of the metamorphic rocks. Finally, as  
 143 the natural case and the experiments compare rela-  
 144 tively well, we tentatively deduce from the numerical  
 145 analysis the most likely range of conditions that pre-  
 146 vailed in the Cyclades domain at the onset of, and  
 147 during, Aegean extension.

148  
 149  
 150 **Numerical modelling**

151 *Initial and boundary conditions*

152  
 153 Two series of numerical experiments have been carried  
 154 out to determine the conditions for development  
 155 of MCCs and particularly sequential development of  
 156 MCCs, as a function of initial crustal thickness,  
 157 thermal structure and boundary velocity.

158 The model geometry consists of a rectangular  
 159 box (500 × 150 km) composed of a continental

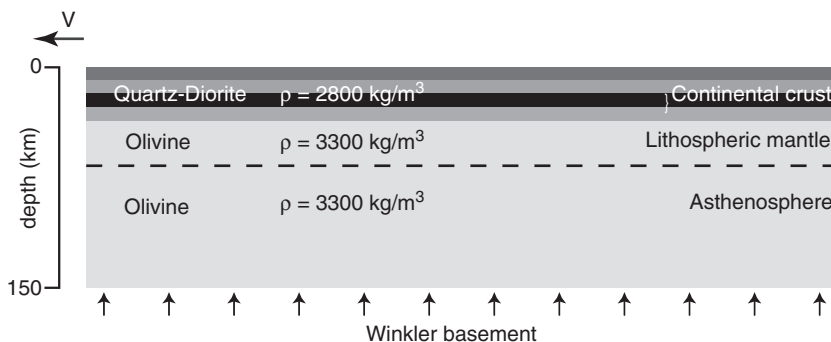
160 crust, a lithospheric mantle and an asthenosphere  
 161 with brittle–elasto–ductile properties (Fig. 2). The  
 162 numerical grid consists of 250 × 75 quadrilateral  
 163 bilinear elements (2 × 2 km). Each element is sub-  
 164 divided into two pairs of triangular sub-elements  
 165 to avoid meshlocking (Cundall 1989). The mesh is  
 166 randomly non-regular (random distribution of the  
 167 nodes) and contains neither an anomaly in structure  
 168 nor a seed that would force deformation to localize  
 169 at a given site. The continental crust has an average  
 170 composition of quartz-diorite with a density of  
 171 2800 kg m<sup>-3</sup> (Table 1). The crust is divided into  
 172 four colour marker layers to provide for a good  
 173 visual tracing of the developing structures. The  
 174 lithospheric mantle and the asthenosphere have  
 an average composition of olivine with a density of  
 3300 kg m<sup>-3</sup> (Table 1). Each numerical  
 element is assigned a specific material phase  
 which is defined by density and thermal and  
 rheological parameters.

The initial temperature field is defined by a  
 surface temperature fixed at 0 °C and a temperature  
 of 1330 °C at the base of the lithosphere. The lateral  
 thermal boundary conditions inhibit heat flow  
 across vertical boundaries of the box (no heat  
 exchange with the surrounding region).

Extension of the entire lithosphere is necessarily  
 dependent on displacements applied at plate bound-  
 aries. Horizontal displacement with constant velocity  
 is applied to the left boundary of the box (Fig. 2). The  
 opposite boundary is fixed. Other boundary condi-  
 tions of the numerical box are a free surface at  
 the top of the box and a pliable Winkler basement  
 at the bottom, which supposes free slip along both  
 surfaces. The vertical normal stresses are proportional  
 to the vertical displacement of the bottom boundary  
 (Burov & Cloetingh 1997). Hydrostatic forces  
 ensure local isostatic compensation.

*Numerical method*

The code PAR(A)OVOZ solves mechanical and  
 thermal equilibrium equations in a large strain  
 mode. This thermo-mechanical code based on



172  
 173  
 174 **Fig. 2.** Model setup used for the numerical experiments.

**Table 1.** Variables and parameters used in the experiments

Variables	Values and Units	Comments
Initial crustal thickness	30, 35, 40, 45, 50, 55, 60 km	Continental crust
Boundary velocity $v$	1, 1.3, 1.6, 2, 2.3, 2.6, 3 $\text{cm}\cdot\text{yr}^{-1}$	Applied on left side (see Fig. 2)
Depth of the thermal lithosphere	60, 80, 100, 120 km	Applied geotherms
Parameters	Values and Units	Comments
Temperature at the base of the lithosphere	1330 $^{\circ}\text{C}$	
Power law constant $A_1$	$1.26 \times 10^{-3} \text{MPa}^{-n}\cdot\text{s}^{-1}$	Quartz-diorite (crust)
Power law constant $n_1$	2.4	Quartz-diorite (crust)
Creep activation energy $E_{a1}$	219 $\text{kJ}\cdot\text{mol}^{-1}$	Quartz-diorite (crust)
Power law constant $A_2$	$7 \times 10^4 \text{MPa}^{-n}\cdot\text{s}^{-1}$	Olivine (mantle)
Power law constant $n_2$	3	Olivine (mantle)
Creep activation energy $E_{a2}$	520 $\text{kJ}\cdot\text{mol}^{-1}$	Olivine (mantle)
Density $\rho_1$	2800 $\text{kg}\cdot\text{m}^{-3}$	Crust
Density $\rho_2$	3330 $\text{kg}\cdot\text{m}^{-3}$	Mantle
Thermal conductivity $k_1$	2.5 $\text{W}\cdot\text{m}^{-1}\cdot\text{K}^{-1}$	Crust
Thermal conductivity $k_2$	3.3 $\text{W}\cdot\text{m}^{-1}\cdot\text{K}^{-1}$	Mantle
Coefficient of thermal expansion	$3 \times 10^{-5} \text{K}^{-1}$	
Internal heat production at surface $H_s$	$10^{-9} \text{W}\cdot\text{kg}^{-1}$	
Specific Heat $C_p$	$10^3 \text{J}\cdot\text{kg}^{-1}\cdot\text{K}^{-1}$	

FLAC<sup>®</sup> and PARAVOZ v3 (Cundall 1989; Poliakov *et al.* 1993) is a mixed finite-difference/finite element, fully explicit, time-marching Lagrangian algorithm, and has been described in several previous publications (Poliakov *et al.* 1993; Burov & Guillou-Frottier 1999, 2005; Burov & Poliakov 2001, 2003; Le Pourhiet *et al.* 2004). The description here will be limited to basic features.

The code solves the conservation equations for energy, mass and momentum:

$$\frac{\partial \rho}{\partial t} + \frac{\partial}{\partial x_i}(\rho v_i) = 0, \quad (1a)$$

where  $v$  is velocity and  $\rho$  is density, with the Newtonian equation of motion in the continuum mechanics approximation:

$$\frac{\rho \partial v_i}{\partial t} - \frac{\partial \sigma_{ij}}{\partial x_j} - \rho g_i = 0, \quad (1b)$$

$$\frac{D\sigma}{Dt} = F(\sigma, \mathbf{u}, \Delta \dot{\mathbf{u}}, \dots, T \dots), \quad (1c)$$

where  $t$  is time,  $g$  is acceleration due to gravity,  $\mathbf{u}$  is the displacement vector,  $T$  is temperature,  $F$  is the functional relationship,  $D$  is material derivative and  $\sigma$  is Lagrangian stress. This equation is coupled with constitutive and heat transport equations:

$$K \nabla^2 T - \rho C_p \frac{\rho T}{\partial t} + H_r = \rho C_p \mathbf{v} \cdot \nabla T \quad (2)$$

where  $\mathbf{v}$  is the velocity vector,  $C_p$  is the specific heat,  $k$  is the thermal conductivity and  $H_r$  is the internal heat production per unit volume. The Boussinesq

approximation is used in the equation of state to account for body forces due to thermal expansion:

$$\rho = \rho_0(1 - \alpha(T - T_0)), \quad (3)$$

where  $\alpha$  is the coefficient of thermal expansion (Table 1). Radiogenic heating is taken into account (Table 1). The right-hand side of equation (2) is calculated directly from equation (1), whilst the left-hand side is computed using a separate numerical scheme. A dynamic relaxation technique, based on the introduction of artificial inertial masses in the dynamic system (Cundall 1989), is used to increase the internal time step and accelerate the solution of the governing equations (1).

The Lagrangian method allows the use of a small strain formulation for large strain problems because the mesh is able to move and deform with the material. At each time step, the new positions of the grid nodes are calculated from the current velocity field and updated in large strain mode accounting for the rotation of principal stress axes using Jauman's co-rotational correction:

$$\begin{cases} \omega_{ij} = \frac{1}{2} \left\{ \frac{\partial u_i}{\partial x_j} - \frac{\partial u_j}{\partial x_i} \right\} \\ \sigma_{ij}^{corrected} = \sigma_{ij}^{small\ strain} + (\omega_{ik} \sigma_{kj} - \sigma_{ik} \omega_{kj}) \Delta t \end{cases} \quad (4)$$

In quasi-static mode, the algorithm uses artificial inertial masses to suppress inertial effects and accelerate the computations (Cundall 1989). PAR(A)O-VOZ also deploys a dynamic remeshing scheme,

233 which makes it possible to model very large  
234 displacements.

235 Each grid element simultaneously handles three  
236 rheological terms: brittle, elastic and ductile; thus  
237 the local deformation mode may change from dom-  
238 inantly brittle to dominantly ductile or elastic,  
239 depending on mechanical and temperature condi-  
240 tions. Material parameters for ductile creep are  
241 obtained from Hansen & Carter (1982) for quartz  
242 diorite and Goetze (1978) for olivine (Table 1).

243 The brittle (plastic) behaviour is described by the  
244 experimental Byerlee's law (Byerlee 1978) which is  
245 reproduced by non-associative Mohr–Coulomb  
246 plasticity with a friction angle  $\phi = 30^\circ$ , cohesion  
247  $C_0 = 20$  MPa and dilatation angle  $\psi = 0^\circ$  (Gerbault  
248 **Q1** *et al.* 1998, 1999):

$$249 \quad |\tau| = C_0 - \sigma_n \tan \phi, \quad (5)$$

251 where  $\tau$  is shear stress and  $\sigma_n$  is normal stress.  
252 Plastic failure occurs if the two following conditions  
253 are satisfied; shear failure criterion  $f = \tau_{11}^* + \sigma_1^*$   
254  $\sin \phi - C_0 \cos \phi = 0$  and  $\partial f / \partial t = 0$  (Vermeer &  
255 de Borst 1984). In 2D formulation,  $\tau_{11}^* =$   
256  $\sqrt{(\tau_{11} - \tau_{22})^2 / 4 + \tau_{12}^2}$  and  $\sigma_1^* = (\sigma_{11} + \sigma_{22}) / 2$ .  
257 In terms of principal stresses, the equivalent of  
258 the yield criterion (5) is:  $\sigma_1 - \sigma_3 = -\sin \phi$   
259  $(\sigma_1 + \sigma_3 - 2C_0 / \tan \phi)$ .

260 The elastic behaviour is described by the linear  
261 Hooke's law:

$$262 \quad \varepsilon_{ij} = E^{-1} \sigma_{ij} - \nu E^{-1} \sigma_{kk} \delta_{ij}, \quad (6)$$

265 where repeating indexes mean summation and  $\delta$   
266 is Kronecker's operator. The values for the elastic  
267 moduli are  $E = 80$  GPa (Young's modulus) and  
268  $\nu = 0.25$  (Poisson's ratio) (Turcotte & Schubert  
269 2002).

270 The viscous (ductile) behaviour is described by  
271 an experimental uni-axial power law relationship  
272 between strain rate and stress (Kirby & Kronenberg  
273 1987; Ranalli 1987):

$$274 \quad e_{ij}^d = A(\sigma_1 - \sigma_3)^n \exp(-H/RT), \quad (7)$$

276 where,  $H = E_a + PV$ ,  $e_{ij}^d$  is the shear strain rate  
277 tensor,  $T$  is the temperature in K,  $\sigma_1$  and  $\sigma_3$  are the  
278 principal Cauchy stresses (compression is negative),  
279  $P$  is the pressure,  $V$  is the activation volume.  $A$ ,  $H$ ,  
280  $E_a$ , and  $n$  are the material constants (Table 1) and  
281  $R$  is the universal gas constant. The effective vis-  
282 cosity  $\mu_{eff}$  for this law is:

$$283 \quad \mu_{eff} = e_{ij}^{d(1-n)/n} A^{-1/n} \exp(H/nRT)^{-1}. \quad (8)$$

286 For non-uniaxial deformation, the uniaxial relation-  
287 ship (7) is converted to a triaxial form using the  
288 invariant of strain rate  $e_{ij}^d = [Inv_{II}(e_{ij}^d)]^{1/2}$  and geo-  
289 metrical proportionality factors (e.g. Burov *et al.*  
290 2003). This is needed because the rotations due to

deformation can be large, and hence the invariant  
form of strain tensor has to be used:

$$\mu_{eff} = e_{II}^{d(1-n)/n} (A^*)^{-1/n} \exp(H/nRT)^{-1}, \quad (9)$$

where  $A^* = \frac{1}{2} A_0 \cdot 3^{(n+1)/2}$ .

The general constitutive viscoplastic model of  
the code is characterized by a visco–elasto–  
plastic deviatoric behavior and an elasto–plastic  
volumetric behaviour, with the following strain  
rate partitioning ( $M =$  Maxwell,  $P =$  'Plastic'):

$$\dot{\varepsilon}_{ij} = \dot{\varepsilon}_{ij}^M + \dot{\varepsilon}_{ij}^P \quad (10)$$

The visco-elastic and plastic strain-rate components  
are thus assumed to act in series. The visco-elastic  
constitutive law corresponds to a Maxwell compo-  
nent, and the plastic constitutive law corresponds  
to the above-described Mohr–Coulomb model. In  
this implementation, the new global stress compo-  
nents are calculated, assuming that the principal  
directions have not been affected by the occurrence  
of plastic flow.

## Numerical experiments

### *Exploring the conditions for MCC-type extension*

To establish the initial and boundary conditions at  
the onset of extension, a series of experiments has  
been performed in order to encompass end-member  
situations of continental extension.

Experiments on the effects of initial crustal  
thickness and initial geotherms (determining the  
initial depth of the 1330 °C isotherm) have been  
carried out. Twenty-eight experiments have been  
performed with initial crustal thicknesses of 30 to  
60 km and initial thermal lithospheric thickness of  
60 to 120 km (Table 1). A constant horizontal dis-  
placement is applied at the left vertical boundary  
with  $v = 2.0$  cm/a for each of these simulations.  
Figure 3a shows the initial geotherm and strength  
profile of the experiments with an initial crustal  
thickness of 30, 44 and 60 km and an initial depth  
of the 1330 °C isotherm at 60, 80, 100 and  
120 km. The classification of three basic domains  
(Fig. 3b) has been made on account of the first  
type of structure observed in the experiments  
(during the first *c.* 20 Ma of extension). They are  
characterized by: (i) the formation of ocean floor;  
or (ii) the development of MCCs (considering that  
the main features defining a MCC are the exhuma-  
tion of middle to lower crustal rocks, a detachment  
zone at the surface, and a flat Moho at depth); or  
(iii) a combination of these two processes (transi-  
tional mode). The experiments identified with

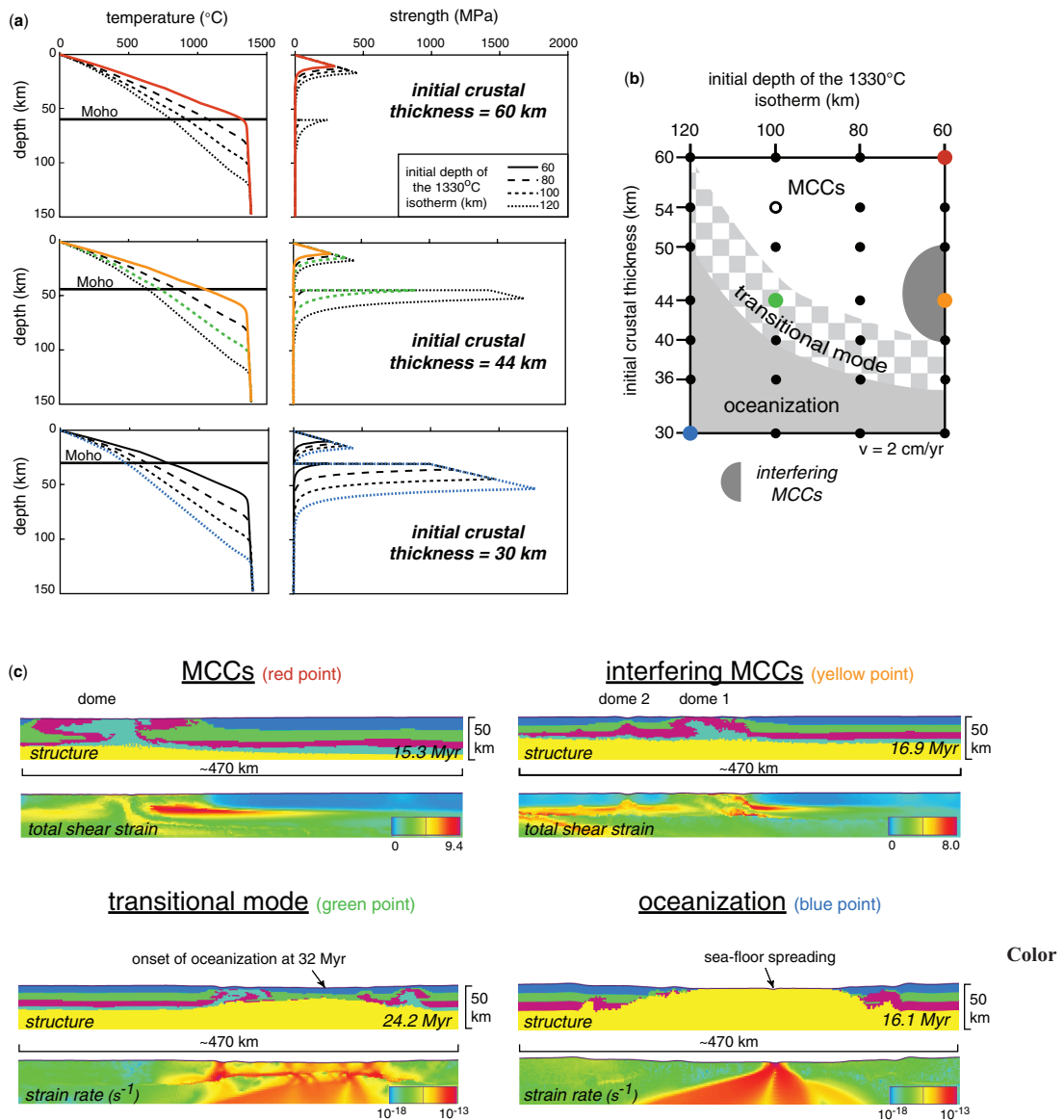


**Fig. 3.** Main results of the first set of numerical experiments, all performed with a boundary velocity of 2.0 cm/a. (a) Initial geotherm and lithosphere strength profile for a selection of experiments with an initial crustal thickness of 30, 44 and 60 km. (b) Distribution of the various modes of extension obtained in a series of 28 experiments (large dots) in a graph combining the initial crustal thickness with the initial depth of the thermal lithosphere (depth of the 1330 °C isotherm). (c) Snapshots of four experiments illustrating the different modes of extension.

colour dots in Figure 3b are shown with the same colours in Figure 3a. Figure 3c shows snapshots of these specific experiments, illustrating the general MCCs mode, the interfering MCCs mode, the transitional mode and the oceanization mode.

The oceanization mode (blue marker) is characterized by a strong necking of the entire continental crust, which results in sea-floor spreading when

break-up occurs (Fig. 3c). This mode implies a high strength of the lithospheric mantle (Fig. 3a).

The MCCs domain identified in Figure 3b displays variable characteristics. Most experiments show the development of several MCCs during extension. Depending on the initial and boundary conditions, the MCCs display a large range in size and amounts of exhumation. This domain can be

349 subdivided into two subdomains, corresponding to  
 350 two modes of extension, with either independent  
 351 or interfering domes. The interfering MCCs mode  
 352 (yellow marker) is obtained for a restricted set of  
 353 conditions, with an initial thickness of the thermal  
 354 lithosphere of *c.* 60 km and an initial crustal thick-  
 355 ness between 40 and 50 km. A detailed description  
 356 of this mode is given in the next section.

357 The non interfering MCCs mode is more  
 358 common (Fig. 3b). An example is given in  
 359 Figure 3c (red marker), which shows the develop-  
 360 ment of a single huge dome. Other experiments  
 361 show the development of several far-distant domes  
 362 that do not interfere with one another. Such an  
 363 experiment is illustrated in Figure 4 (identified  
 364 with an open dot in Fig. 3b). The first timeslice  
 365 (10.1 Ma) shows the exhumation of a first MCC  
 366 (dome 1) and the incipient development of a  
 367 graben (graben 2) which later evolves into a new  
 368 MCC (dome 2 in timeslices 15.2 and 20.1 Ma).  
 369 The graben is located away from the first dome  
 370 (*c.* 165 km) and related shear zones (SZ1 and  
 371 SZ2). While the second dome develops, new shear  
 372 zones form (SZ3 and SZ4). The tips of SZ2 and  
 373 SZ3 are in mutual contact but the two shear zones  
 374 do not overlap, therefore SZ3 does not reactivate  
 375 SZ2. Similar features are obtained for the relations  
 376 between dome 2 and dome 3 and between SZ4 and  
 377 SZ5 (Fig. 4). We refer to this situation as a case  
 378 where the MCCs remain independent, in the sense  
 379 that there is no kinematic interference between  
 380 them. Nevertheless, a dynamic interference is  
 381 likely, because the development of a first dome  
 382 reduces the potential of lower crustal flow, thereby  
 383 limiting the development of subsequent domes.

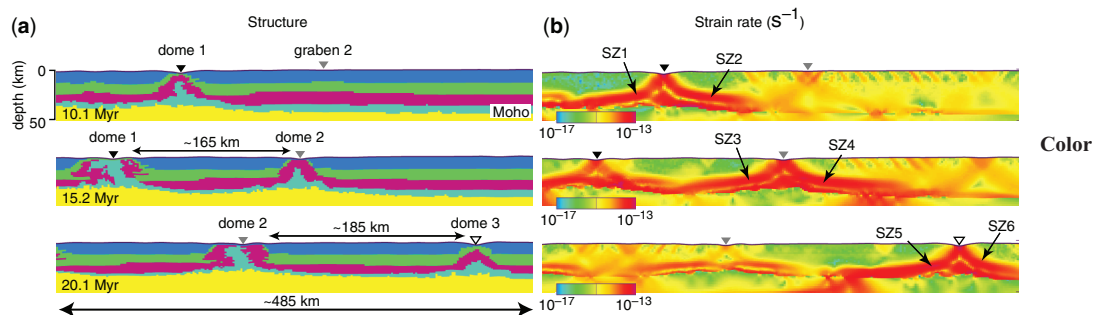
384 The general MCCs mode is obtained for condi-  
 385 tions favouring the existence of a weak lower  
 386 crust, with either a thick crust or a thin lithosphere  
 387  
 388  
 389

(both conditions leading to high temperature condi-  
 tions at the Moho) or both (Fig. 3b). In the  
 extreme case (red marker), a huge MCC is obtained  
 (Fig. 3c). As seen in Figure 3a, a low-strength  
 sub-Moho mantle appears to be another necessary  
 condition for obtaining a MCCs mode of extension  
 with a flat Moho, as already suggested by Buck  
 (1991). This agrees with the results obtained in a  
 different parametric study (with a boundary velocity  
 of 0.66 cm/a) by Tirel *et al.* (2008), who found that  
 the development of MCCs requires an initial Moho  
 temperature of 800 °C or higher. At these tempera-  
 tures, both the sub-Moho mantle and the lower  
 crust have low strengths and viscosities of the  
 order of  $10^{19}$ – $10^{21}$  Pa.s. Figures 3a and 3b suggest  
 that a sub-Moho mantle with a strength of only  
*c.* 250 MPa is enough to prevent the formation of  
 MCCs. In addition, to obtain a MCCs mode of  
 extension, an initial crustal thickness of at least  
 40 km seems required (Fig. 3b). In a thinner crust,  
 lower crustal flow is probably hampered by the  
 limited amount of material able to flow.

Finally, the transitional mode (green marker) is  
 characterized by the development of MCCs of moder-  
 ate size closely followed by the formation of an  
 ocean floor (Fig. 3c), or by the formation of  
 pseudo-MCCs showing a substantial rise of the  
 Moho, eventually followed by the formation of  
 an ocean.

*Experiments with interfering MCCs*

The conditions leading to interfering MCCs have  
 been further investigated through a second series  
 of experiments, in order to determine the effects of  
 the initial crustal thickness and the boundary vel-  
 ocity (Table 1) on the three main properties directly  
 comparable with geological and geophysical data;



390  
 391  
 392  
 393  
 394  
 395  
 396  
 397  
 398  
 399  
 400  
 401  
 402  
 403 **Fig. 4.** Results obtained for an experiment with an initial crustal thickness of 54 km, an initial depth of the 1330 °C  
 404 isotherm at 100 km, and a boundary velocity of 2.0 cm/a (cf. the open dot in Fig. 3b). This experiment illustrates the  
 405 general MCCs mode of extension, in which several MCCs form but remain far-distant, so that they do not interfere. The  
 406 successive timeslices are dated with respect to the onset of extension. The triangles above the surface are markers  
 helping to locate structures from one panel to the other.

the width of the dome, the duration of dome development and the final Moho depth. The three first experiments leading to interfering MCCs have been performed with initial crustal thicknesses of 40, 44 and 50 km, an initial thermal lithospheric thickness of 60 km and a boundary velocity of 2.0 cm/a (Table 1) (Fig. 3b). In addition, six experiments have been carried out with an initial crustal thickness of 44 km, an initial thermal lithospheric thickness of 60 km and boundary velocities of 1.0, 1.33, 1.66, 2.33, 2.66 and 3.0 cm/a (Table 1). Three of these experiments show interfering

MCCs. In all the experiments displaying interfering MCCs, the domes develop in sequence (one after the other). The results of the two series of experiments are shown and discussed below.

*Description of two experiments.* The sequential development of interfering MCCs is illustrated in Figure 5 with two experiments having an initial crustal thickness of 44 km, an initial depth of the 1330 °C isotherm of 60 km and a boundary velocity of 2.0 cm/a (Type 1 experiment, corresponding to the yellow marker in Fig. 3) or 2.33 cm/a (Type 2

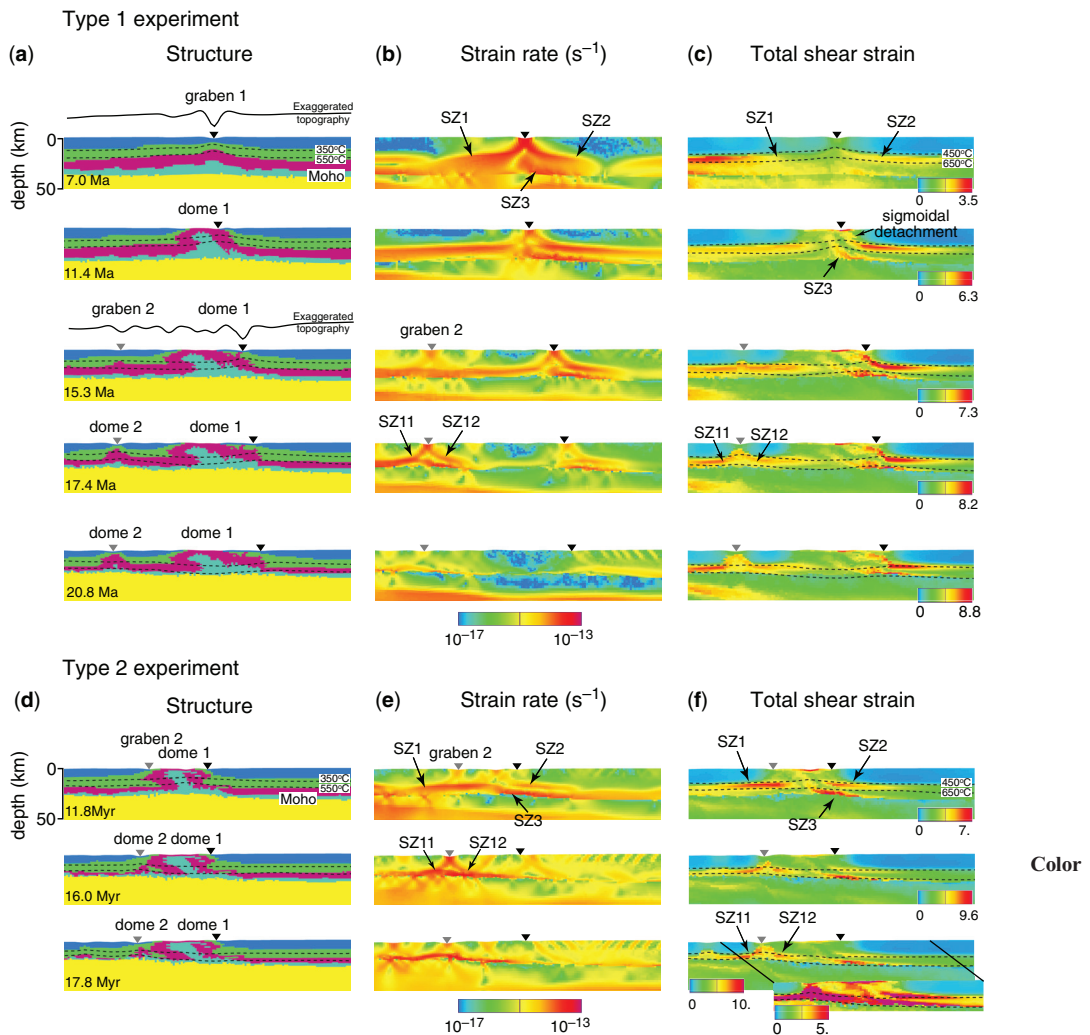


**Fig. 5.** Results obtained for two experiments with an initial crustal thickness of 44 km, an initial depth of the 1330 °C isotherm at 60 km, and a boundary velocity of 2.0 cm/a (Type 1, cf. the yellow dot in Fig. 3b) or 2.3 cm/a (Type 2). These experiments illustrate the interfering MCCs mode of extension. The successive timeslices are dated with respect to the onset of extension. The triangles above the surface are markers helping to locate structures from one panel to the other. A topographic profile with a vertical exaggeration of 10 is represented in (a) above the timeslices 7.0 and 15.3 Ma.

465 experiment). These two experiments document a  
466 similar process, differing only in terms of distance  
467 between adjacent MCCs. The model setup is  
468 shown in Figure 2. At the onset of extension, the  
469 effective viscosity of the sub-Moho mantle and the  
470 lower crust is very low ( $10^{19}$ – $10^{20}$  Pa.s) and the  
471 two layers are coupled. The experiment of type 1  
472 has been chosen to illustrate the entire process of  
473 exhumation. Since the process is the same, only  
474 the last stages of the second experiment are  
475 shown. The images have been truncated in order  
476 to focus on the most important crustal structures.  
477 Only a window of  $280 \times 50$  km is shown. In  
478 addition to those visible in Figure 5, other domes  
479 are exhumed during each experiment, but do not  
480 interfere with one another. These independent  
481 MCCs are not shown here, nevertheless, they bear  
482 similar characteristics as those seen in Figure 4.  
483 The ages are relative to the onset of extension.

484 The first timeslice of Type 1 experiment, at  
485 7.0 Ma (Fig. 5a, b, c), shows a simultaneous localiza-  
486 tion of strain in the upper and lower crust. The  
487 structure defines a symmetrical graben in the  
488 brittle crust (graben 1) and two major conjugate  
489 shear zones (SZ1 and SZ2) in the ductile middle  
490 crust (Fig. 5b, c). The two shear zones are flat-lying,  
491 located at depths around 22–25 km. A third shear  
492 zone (SZ3) develops below SZ2 at the Moho inter-  
493 face (Fig. 5b, c). At this stage, the ductile middle-  
494 lower crust already rises toward the surface  
495 (Fig. 5a).

496 The second timeslice, at 11.4 Ma, shows the  
497 development of an asymmetric dome (dome 1) fol-  
498 lowing the extreme thinning of the upper crust  
499 (Fig. 5a). Middle and lower crustal levels have  
500 reached the surface and active deformation is local-  
501 ized mainly on the right side of the dome  
502 (Fig. 5b, c). SZ2 displays a sigmoidal shape of  
503 three parts: flat on the dome top, steeply dipping  
504 on the right dome limb and flat again in the lower  
505 crust (Fig. 5c). This forms the detachment shear  
506 zone observed at the roof of the metamorphic  
507 dome. The isotherms rise asymmetrically with  
508 respect to the dome apex (Fig. 5a), which confirms  
509 the localization of deformation along SZ2. The  
510 right side of the dome now forms the zone of  
511 lowest topography, and is a likely locus for a supra-  
512 detachment basin superimposed on initial graben  
513 formation. SZ3 shows a shape similar to SZ2 but  
514 does not reach the surface. SZ3 is near-horizontal  
515 at the Moho and steeply inclined inside the dome.  
516 While still active, SZ1 has not significantly  
517 changed in shape or depth since the beginning  
518 of deformation.

519 At 15.3 Ma, dome 1 continues to develop with a  
520 recumbent-like fold shape (Fig. 5a). Flattening of  
521 this structure is also observed in the shape of SZ2  
522 and SZ3 (Fig. 5c). Nevertheless, the strain rate

pattern remains stable (Fig. 5b). Further left, a  
slight rise of the lower crust is observed (Fig. 5a),  
accompanied by a slight rise of SZ1 (Fig. 5c). It is  
related to localization of deformation in the brittle  
crust leading to formation of a second graben  
(graben 2, Fig. 5a, b). It is noteworthy that, in this  
experiment, graben 2 is located right above one of  
the previously formed shear zones (SZ1), at vari-  
ance with the situation in those experiments that  
generated independent MCCs (Fig. 4b). In all the  
experiments showing a sequential development of  
domes, the smaller secondary dome originates  
from necking of the upper crust in a stage where  
the crustal thickness stands between 28 and 32 km  
and the Moho temperature is between 750 and  
810 °C.

At 17.4 Ma, the shape of dome 1 has not signifi-  
cantly changed and the strain rate pattern indicates  
that active deformation has strongly decreased  
there, especially along SZ1 (Fig. 5a, b). A second  
dome (dome 2) begins to develop symmetrically,  
dragging SZ1 toward the surface (Fig. 5c). SZ1 is  
splitted into two branches located on both limbs of  
dome 2 (SZ11 and SZ12, Fig. 5b, c). SZ12 reactiv-  
ates SZ1 with an opposite, top-to-the-right sense  
of shear.

At 20.8 Ma, the isotherms have deepened and  
flattened, documenting advanced cooling of both  
domes (Fig. 5a). The strain rate pattern indicates  
an overall strong decrease in active deformation  
(Fig. 5b).

The initial conditions in Type 2 experiment are  
the same as before except for the boundary velocity,  
which is slightly higher. Only the three last stages  
are shown here (Fig. 5d, e, f). The second dome is  
smaller and develops closer to the first dome than  
in the previous experiment. As a result, there is no  
lid of upper crust left between the two domes. Other-  
wise the two experiments show similar character-  
istics. In both cases, the Moho remains  
sub-horizontal throughout the extensional process  
and reaches the depth of *c.* 25 km when the exhuma-  
tion of MCCs has ended.

*Analysis of the two experiments.* Figure 6 depicts  
schematically the sequential development of inter-  
fering MCCs, based on the results shown in  
Figure 5. As previously discussed by, for example  
Tirel *et al.* (2004a, 2008), the development of  
MCCs may be characterized by two main stages:  
(1) upper crustal necking (graben formation)  
accompanied by the formation of flat-lying conju-  
gate shear zones in the lower crust (Fig. 6a);  
followed by (2) exhumation of the dome (amplifica-  
tion and widening) owing to the connection, at  
mid-crustal depths, of the faulted graben with one  
of the lower crustal shear zones, forming the main  
detachment zone (Fig. 6b).

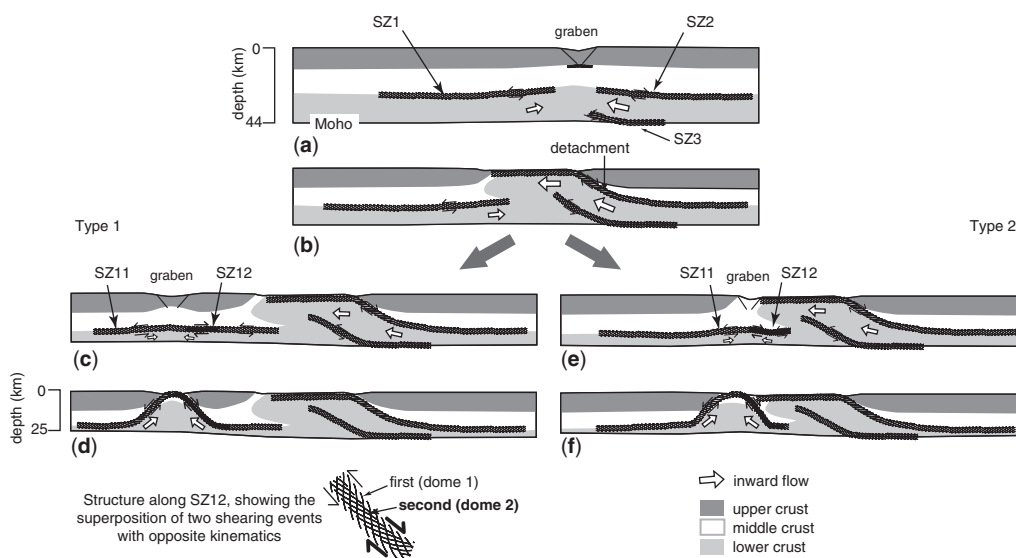


**Fig. 6.** Sketch based on the results shown in Figure 5, depicting the process of sequential development of interfering MCCs.

Upper crustal necking results in a reduction of the vertical lithostatic load, which induces a horizontal pressure gradient. Due to this gradient, the most ductile material at depth flows horizontally toward the area of necking. We use the term inward flow to describe this feature (cf. Brun & van den Driessche 1994). Inward flow is commonly described in MCC models as a process responsible for a flat Moho geometry (Block & Royden 1990; Wdowinski & Axen 1992; Wernicke 1992; Brun & van den Driessche 1994; Tirel *et al.* 2004a, 2008; Gessner *et al.* 2007). In our experiments, horizontal flow of the lower crust occurs over distances several times larger than the width of the dome and is responsible for the development of horizontal shear zones. Two convergent channel flows are systematically obtained, resulting in two conjugate flat-lying shear zones (SZ1 and SZ2; Figs 5 & 6). High strain intensities are also found within SZ3, which follows the Moho but bends upward beneath the dome apex. This particular shape is associated with fast and relatively focused rise of lower crustal material during dome amplification.

Still in the experiments, shearing due to inward flow occurs at the interface between a lower part of the crust where rocks are weak enough to flow pervasively, and an upper part where rocks are too strong to undergo significant deformation (while SZ3, at greater depth, is a mirror effect along the Moho boundary). This interface has a certain thickness, corresponding to the domain where rocks can undergo ductile shearing, in between the isotherms

450 and *c.* 650 °C (Fig. 5c). This thickness depends also partly on the resolution of the experiments. As seen in Figure 3a, we obtain a temperature of the transition between ductile and brittle behaviours of *c.* 300 °C for quartz diorite, which is the rock type we have chosen to represent the crust as a whole (note that, in our experiments, this temperature is not imposed but arises from the combination of the brittle and ductile rheological laws). Thus, in the simulations, shearing due to inward flow occurs at significantly greater depths than the ductile–brittle transition (that is, at temperatures at least *c.* 150 °C higher, corresponding to a difference in depth of about 6 km in the case of Type 1 experiment, cf. the yellow marker of Fig. 3). On the one hand, this difference is consistent with the shape of the strength profiles shown in Figure 3a, in which the brittle–ductile transition coincides with a peak in strength. In this case, shearing along the roof of a lower crustal channel may be expected to occur more readily significantly below the brittle–ductile transition. This agrees with the observation that, in Figure 3a, the temperature of 450 °C coincides with the point of inflexion along the ductile segment of the strength profile, hence marking a relatively abrupt transition between the strong ductile crust, above, and the weak one, below. On the other hand, several authors have argued that rocks immediately beneath the ductile–brittle transition may represent a low in the strength profile of the crust after a certain amount of strain is accumulated, so that this level could be used as a décollement (e.g. Handy

1989; Gueydan *et al.* 2004). If so, then it is conceivable that the roof of the shear zone overlying the lower crustal channel may coincide with the ductile–brittle transition, a situation that our experiments cannot feature. It is also worth stating that our model setup considers the crust as homogeneous; a compositionally layered crust may result in a distinct picture, with a different depth distribution of the shear zones.

In all experiments with interfering MCCs, the second MCC follows the same two-stage development as described above. Figures 6c and 6d and Figures 6e and 6f depict the results obtained in the Type 1 and Type 2 experiments, respectively, the main difference being the distance between the two domes. In both cases, localization of the second graben occurs right above SZ1 which formed during the development of the first dome. This preexisting structure is dragged toward the surface during the amplification stage of the second dome. In addition, renewed inward flow leads SZ1 to be reactivated with a similar sense of shear on the left dome limb (SZ11) but with an opposite sense of shear on the right dome limb (SZ12). This, in turn, hampers inward flow and temperature advection toward dome 1, favouring its cooling and increase in strength (cf. Fig. 5a, b). Widening of the second dome is limited because of the strong crustal thinning already achieved. Since the second dome remains small, shearing along SZ12 probably involves less strain than earlier, kinematically opposite shearing along SZ1 involves (see also Fig. 5b). Hence, relics of the first event should be found along the shear zone. In the end, the strength of the crust is too high to enable lower crustal flow any longer. If extension is to continue due to unchanged boundary conditions, it must proceed without MCCs being further developed. Until that stage, the Moho remains almost flat throughout the exhumation process. This is due to coherent ductile deformation between the lower crust and the sub-Moho mantle (see also Tirel *et al.* 2008).

*Role of the initial crustal thickness and the boundary velocity.* Figure 7 synthesizes the effects of modifying the initial crustal thickness or the boundary velocity on three measurable aspects of each experiment. The results shown are only for the experiments that yield interfering MCCs. The output parameters are the width of the domes (measured at the surface), the time needed to exhume the first dome (and, combining the domes, the duration of MCC-type extension), and the final depth of the Moho.

The width of the first dome (between 24 and 110 km) and the duration of its exhumation (between 11 and 24 Ma) increase with increasing initial crustal thickness and decreasing boundary

velocity (Fig. 7a, b, c, d). Note that the huge dome obtained for an experiment with a 60 km-thick crust (Fig. 3b, c) is consistent with this trend.

The width of the second dome (between 15 and 30 km) and the duration of its exhumation (between 5 and 8 Ma) are much less variable than they are for the first dome. As quoted in the Description of two experiments' section, in all experiments, the second dome originates from necking of the upper crust in a stage where the crustal thickness lies in a narrow range, between 28 and 32 km. Hence, the width and timing of exhumation of the second dome are not directly related to the initial conditions of the experiment but to those once the first dome has essentially formed. This is consistent with the view that widening of the second dome, which depends on the possibility of renewed inward flow, is limited by the amount of crustal thinning already achieved during the development of the first dome, which itself is a function of the initial crustal thickness. In other words, the ability of the first dome to absorb a large volume of weak lower crust is proportional to the volume initially available, so that the amount of weak material left for the second dome is always nearly the same.

Combining the timing of exhumation of both domes, a duration of MCC-type extension is obtained, ranging between 16 and 32 Ma (Fig. 7c, d). The width of the whole complex made up of two adjacent domes is not plotted here. This width is related to the width of the domes but also to the distance between them. This distance is variable (cf. the difference between Type 1 and Type 2 experiments) but does not show a clear correlation with the initial crustal thickness or the boundary velocity.

After exhumation of the two domes, the Moho interface is always nearly flat. The final Moho depth (between 22.5 and 29 km) increases with increasing initial crustal thickness and with decreasing boundary velocity (Fig. 7e, f).

## Geology of the Cyclades

The above two-dimensional numerical experiments suggest that, for certain conditions, MCCs may develop in sequence during continental lithospheric extension. Extrapolated to a three-dimensional setting, the corresponding region could be characterized by the development of several chains of MCC, each chain trending orthogonal or at a high angle to the direction of extension. Although such a situation may be encountered in several regions worldwide (see Introduction), we will here focus on the Cyclades archipelago because, in our view, this is the area where the existence of subparallel chains of MCC has been best documented so far. In this section, we review the structural and

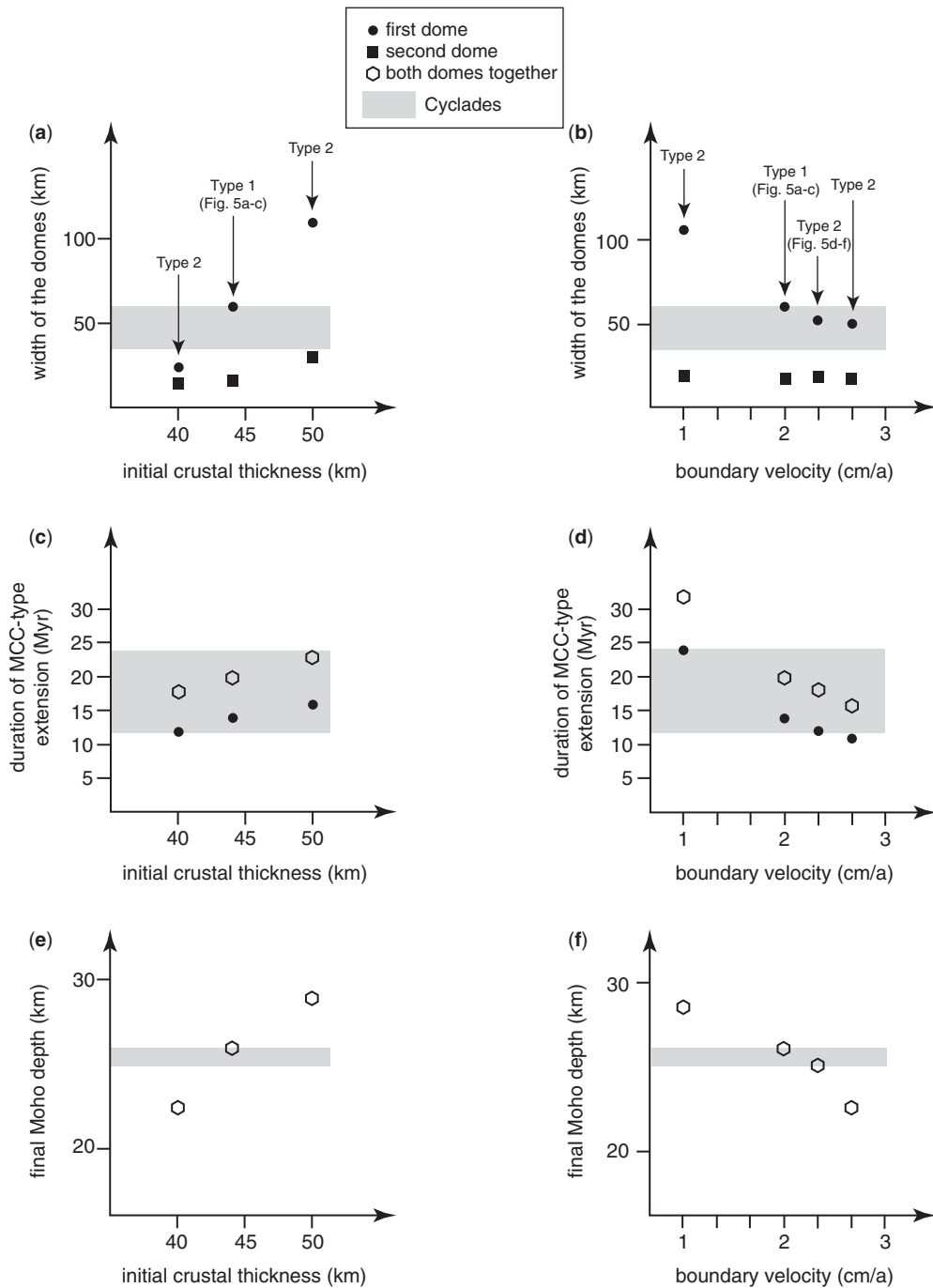


**Fig. 7.** Series of graphs summarizing the effects of modifying the initial crustal thickness (left) or the boundary velocity (right) on the width of the domes (top graphs), the time needed to exhume the first dome (black dot) and, combining the domes, the duration of MCC-type extension (open symbol) (middle graphs), and the final depth of the Moho (bottom graphs). Grey bands represent the range of values in the Cyclades, as deduced from available geological and geophysical data (see the text). More precisely, the grey band in (a) and (b) represents the width range for Naxos and Paros first-generation MCCs, to be compared with the numerical results obtained for the first dome only; the grey band in

697 metamorphic evolution of the Cyclades (see also  
698 Fig. 8), focusing on features that allow comparison  
699 with our numerical results.

700 Since the seminal paper of Lister *et al.* (1984),  
701 many studies have focused on the identification of  
702 extensional detachments and metamorphic core  
703 complexes in the Cyclades (e.g. Urai *et al.* 1990;  
704 Buick 1991; Gautier *et al.* 1993; Gautier & Brun  
705 1994a; Vandenberg & Lister 1996; Forster &  
706 Lister 1999; Jolivet & Patriat 1999; Kumerics  
707 *et al.* 2005; Iglseider *et al.* 2006; Müller *et al.*  
708 2006). During extension, rocks that previously  
709 recrystallized in high-pressure/low-temperature  
710 conditions were exhumed from the conditions of a  
711 greenschist facies or higher grade overprint to the  
712 conditions of brittle deformation. Granitoid intru-  
713 sions also emplaced during extension (e.g. Altherr  
714 *et al.* 1982). Time constraints indicate that these  
715 structures are broadly Miocene in age, most  
716 authors agreeing on the view that they formed  
717 during Aegean ‘backarc’ (or post-orogenic/post-  
718 thickening) extension. Lister *et al.* (1984) initially  
719 proposed that extension was controlled by a single  
720 south-dipping detachment zone on the scale of the  
721 Cyclades archipelago, however subsequent studies  
722 have documented a more complex structural  
723 pattern.

724  
725 *The Cyclades as a coherent domain during*  
726 *Miocene extension*  
727

728 Because the orientation of extension-related stretch-  
729 ing lineations and subsequent normal faults shows a  
730 fairly abrupt change across the archipelago, it is  
731 tempting to subdivide the Cyclades into two  
732 domains. The direction of maximum stretching is  
733 NE–SW to ENE–WSW in the northwestern  
734 islands, and North–South in the southeastern  
735 islands (Gautier & Brun 1994a) as well as on  
736 Ikaria (Kumerics *et al.* 2005). The boundary  
737 between these two domains coincides with a NE–  
738 SW-trending fault zone extending from west of  
739 Ikaria to east of Sifnos, with probably a significant  
740 wrench (dextral) component of movement along it  
741 (Gautier & Brun 1994a; Gautier 1995). This fault  
742 zone has been named the Mid-Cycladic Lineament  
743 (MCL) by Walcott & White (1998). Opposite  
744 rotations across the fault zone, as documented by  
745 palaeomagnetic data on middle Miocene intrusions

on Naxos, Mykonos and Tinos (Morris & Anderson  
1996; Avigad *et al.* 1998), confirm the importance  
of the MCL and are consistent with the view that  
the divergent pattern of lineations seen on the  
scale of the Cyclades relates originally to a  
uniform NNE–SSW direction of stretching  
(Gautier & Brun 1994b; Walcott & White 1998;  
Gautier *et al.* 1999; Jolivet *et al.* 2004). This view  
is also consistent with the pattern of rotations on  
the scale of the whole Aegean region (van Hinsber-  
gen *et al.* 2005b). Gautier & Brun (1994b) suggested  
that a rectilinear horst-and-graben system initially  
occupied the Central Aegean region and underwent  
progressive bending due to radial spreading of the  
Aegean lithosphere. Analogue experiments further  
showed that the presence of a thin layer of sand  
(simulating the brittle behaviour of the upper  
crust) at the top of a spreading sheet is a condition  
sufficient to produce a pattern of oppositely  
rotated blocks separated by a sharp boundary equiv-  
alent to the MCL (Gautier *et al.* 1999). Therefore,  
the MCL can be seen as a structure accommodating  
lateral variations in the rotation field of the Central  
Aegean region during regional extension. In con-  
trast, Pe-Piper & Piper (2006) recently proposed a  
series of palinspastic reconstructions of the  
Aegean domain in which they assume *c.* 100 km  
of sinistral displacement along the MCL during  
the Miocene (from 17 to 5 Ma, mostly). This  
would imply that the Central Aegean region actually  
consists of two domains that were far distant from  
each other during early stages of core complex-type  
extension (Pe-Piper & Piper 2006, Figs 2 & 13).  
However, on account of the similarity of lithologies,  
tectonometamorphic evolution, and timing of exhu-  
mation of rocks on both sides of the MCL, our  
opinion is that the total offset across the MCL  
must be minor, in agreement with Walcott &  
White (1998).

746  
747 *How many MCC and detachment systems*  
748 *in the Cyclades?*

A number of observations imply that several MCCs  
coexist in the Cyclades. Most islands have the geo-  
metry of a metamorphic dome defined by the orien-  
tation of foliations, occasionally also by lithological  
contours, and more rarely by a concentric pattern of  
isograds (Naxos and Paros). On several islands, a

748  
749 **Fig. 7.** (Continued) (c) and (d) represents the duration of MCC-type extension in the Cyclades. The time lags for  
750 exhuming the first dome and the duration of MCC-type extension are given with respect to the onset of post-orogenic  
751 extension. Somehow arbitrarily, the time at which the first dome finishes its exhumation is taken as the time at which the  
752 second dome starts to form. Figure 5a–b shows that their developments may slightly overlap in time (i.e. shearing is still  
753 active along the frontal detachment of the first dome while the second dome rises) but also that far much of the exhumation  
754 of the first dome has occurred before the second dome forms. The time difference between the black dot and the open  
symbol represents the time lags for exhuming the second dome. It shows little variation, between 5 and 8 Ma.

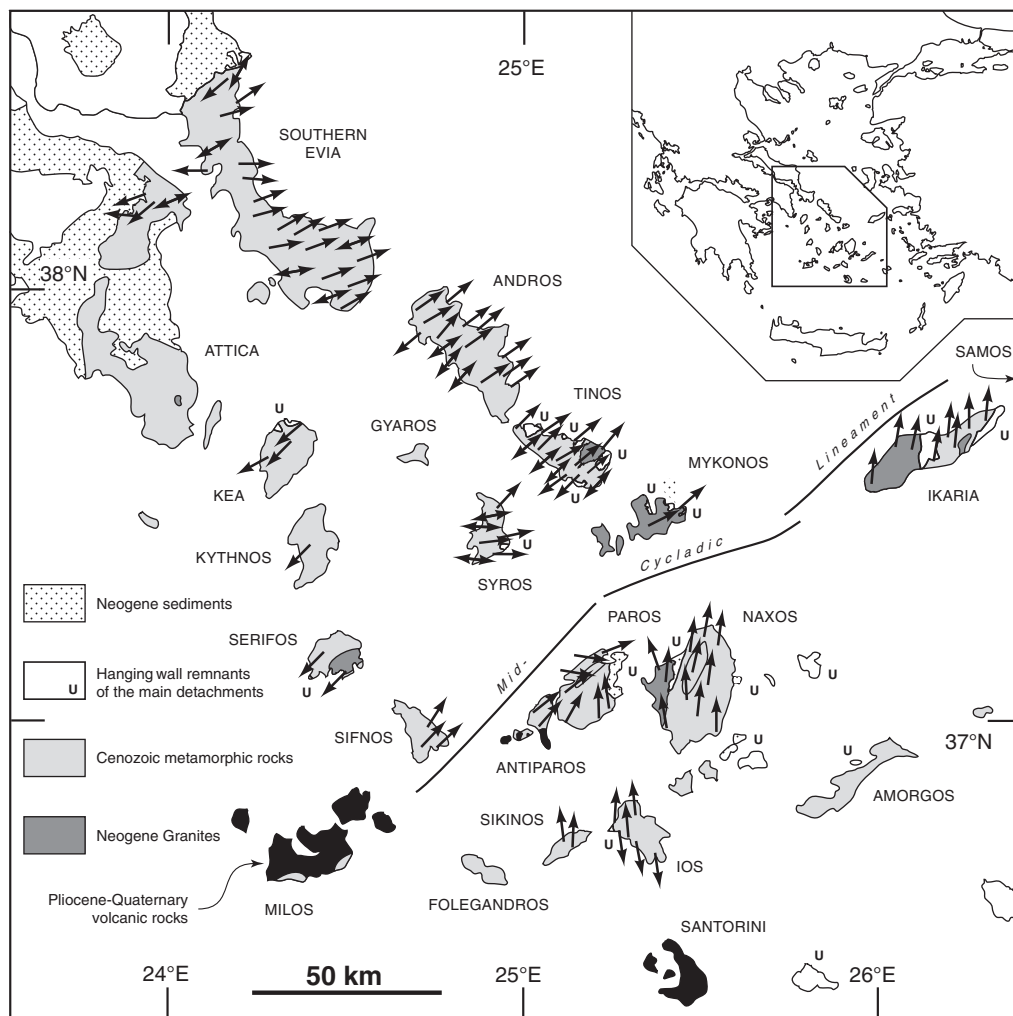


**Fig. 8.** Simplified geological map of the Cyclades archipelago. Arrows indicate the kinematics of extensional shearing during greenschist facies and locally higher temperature metamorphism, subsequent cooling to the conditions of brittle deformation, and within syn-kinematic intrusions. Data after Buick (1991), Gautier *et al.* (1993), Gautier & Brun (1994a, b), Gautier (1995), Vandenberg & Lister (1996), Walcott & White (1998), Jolivet & Patriat (1999), Trotet *et al.* (2001a), Kumerics *et al.* (2005), Iglseider *et al.* (2006) and Grasemann *et al.* (2007).

composite unit made of rocks that experienced no or limited metamorphism during the Cenozoic, rests upon the flanks of the metamorphic dome. The contact between this unit and the underlying metamorphic rocks usually bears the characteristics of an extensional detachment zone having accommodated the exhumation of the footwall rocks starting from the depths of greenschist facies and locally higher temperature metamorphism (e.g. Lister *et al.* 1984; Urai *et al.* 1990; Gautier *et al.* 1993; Gautier & Brun 1994a; Jolivet & Patriat 1999; Jolivet *et al.* 2004; Mehl *et al.* 2005; Müller *et al.*

2006; Grasemann *et al.* 2007). Therefore, each metamorphic dome may be described as a MCC. However, the Cyclades have also experienced Messinian–Quaternary high-angle faulting, with normal faults usually dipping away from the islands (e.g. Angelier 1977a, b; Gautier & Brun 1994a), so that it may be asked whether drag folding along these late faults could alone have produced the dome shape of some of the islands. This is unlikely at least on Naxos, Paros and Ios, where the domes are pronounced and regular (e.g. van der Maar & Jansen 1983; Gautier *et al.* 1993).

813 Occasionally, low-angle normal faults also dissect  
814 the islands and make the identification of a meta-  
815 morphic dome more difficult, like on Syros  
816 (Ridley 1984).

817 A critical question is whether distinct MCCs  
818 found along a section parallel to extension were  
819 initially associated with a single detachment zone,  
820 as Lister *et al.* (1984) suggested, or formed  
821 beneath distinct detachment zones (Gautier &  
822 Brun 1994*b*). Gautier & Brun (1994*a, b*) and  
823 Gautier (1995) argued that, on several islands, a  
824 specific distribution of kinematic indicators could  
825 be seen, like on Tinos, Andros, central southern  
826 Evia, Ios and, to a lesser extent, Syros. They  
827 described the ductile deformation associated with  
828 greenschist facies metamorphism as non-coaxial,  
829 with a top-to-north (or NE) sense of shear in the  
830 northern (or northeastern) part of these islands,  
831 and a top-to-south (or SW) sense of shear in the  
832 southern (or southwestern) part. On Tinos and  
833 Andros, the domain with top-to-SW shearing is  
834 restricted to a few outcrops along the southwestern  
835 coast, so that the corresponding domes appear asym-  
836 metric with respect to the shear sense pattern (i.e.  
837 top-to-NE shearing dominates). According to  
838 Gautier & Brun (1994*a, b*), the sense of shear is  
839 inverted across a *c.* 1 km-wide zone trending sub-  
840 perpendicular to the mean stretching lineation.  
841 Within it, conjugate patterns of shear bands and  
842 symmetric boudinage structures dominate, so that  
843 this zone may be viewed as a narrow domain of  
844 coaxial strain at the transition between two  
845 domains with opposite kinematics. Further investi-  
846 gations on Tinos and Andros led Jolivet & Patriat  
847 (1999) to modify this description (see also Jolivet  
848 *et al.* 2004; Mehl *et al.* 2005). According to these  
849 authors, the coastal outcrops showing top-to-SW  
850 shearing should not be considered as a distinct  
851 entity but belong to a domain of coaxial strain sig-  
852 nificantly wider than previously presumed, beside  
853 the domain showing uniform top-to-NE shearing.  
854 Gautier & Brun (1994*a, b*) interpreted the above  
855 pattern as reflecting the dynamics of the ductile  
856 lower crust in response to isostatic rebound and  
857 dome amplification beneath a contemporaneous  
858 detachment zone (that is, the process of 'inward  
859 flow' discussed herein). A different opinion is  
860 shared by Jolivet & Patriat (1999) and Jolivet  
861 *et al.* (2004), who interpret the juxtaposed  
862 domains of coaxial and non-coaxial strain as reflect-  
863 ing the configuration in the middle crust, around the  
864 brittle-ductile transition zone, during early stages  
865 of extension. With further extension, the main  
866 extensional shear zones of the middle crust evolve  
867 into typical extensional detachments (Jolivet *et al.*  
868 2004). A potential problem with this interpretation  
869 is the presence, in southern Tinos, of a large  
870 klippe (or 'extensional allochthon') of the same unit

that forms the hanging wall of the detachment  
zone in the northeastern part of the island. This  
klippe rests entirely onto the domain of coaxial  
strain defined by Jolivet & Patriat (1999). While  
this feature is normal in the model invoked by  
Gautier & Brun (1994*a, b*) (see also Brun & van  
den Driessche 1994), it is unexpected in that of  
Jolivet & Patriat (1999), even after a large amount  
of displacement is achieved along the detachment  
(cf. Jolivet *et al.* 2004, Fig. 13). Because well pre-  
served eclogites and blueschists are found slightly  
beneath the klippe, and by analogy with the situation  
on Syros (see next section), Trotet *et al.* (2001*a*) and  
Mehl *et al.* (2005) suggested that the intervening  
contact represents an extensional detachment sig-  
nificantly older than that seen in the northeastern  
part of the island (at a distance of only 5 km).  
However, since the rocks in between belong to the  
same footwall unit with low-dipping foliations,  
this hypothesis does not readily solve the problem:  
the contact in the south and the northeastern detach-  
ment occupy the same structural position, therefore  
the former should have been reactivated (if not  
entirely developed) during greenschist facies shear-  
ing along the latter and is most probably connected  
with it. Due to this problematic issue, and on  
account of the numerical results obtained in this  
study, our opinion is that the interpretation of  
Gautier & Brun (1994*a*) remains a viable alternative  
to the one of Jolivet & Patriat (1999).

Regardless, taking into account the report of  
top-to-NE/ENE shearing in northern and eastern  
Syros during greenschist facies metamorphism  
(Gautier 1995; Trotet *et al.* 2001*a*; Rosenbaum  
*et al.* 2002), the domain of coaxial strain in south-  
western Tinos strongly suggests that Tinos and  
Syros islands already coincided with distinct meta-  
morphic domes during that stage of the meta-  
morphic evolution. As a consequence, the Tinos  
detachment and the detachment seen in southeastern  
Syros, bearing a similar hangingwall rock content  
(Maluski *et al.* 1987; Patzak *et al.* 1994), were  
also probably distinct shear zones at that time  
(Gautier & Brun 1994*b*).

By analogy, it can be proposed that three parallel  
detachment systems have developed in the north-  
western Cyclades during Miocene extension,  
coinciding with the three NW-SE-trending chains  
of islands seen at present, namely southern  
Evia-Mykonos, Gyaros-Syros, and Kea-Sifnos  
(Gautier & Brun 1994*a*; Jolivet *et al.* 2004). The  
Evia-Mykonos chain is clearly dominated by  
top-to-NE ductile to brittle shearing, therefore it  
was controlled by a NE-dipping detachment zone.  
In contrast, the kinematics of extensional defor-  
mation are not so clearly asymmetric in the case  
of the Gyaros-Syros chain. While top-to-NE/  
ENE shearing dominates in the eastern part of

871 Syros, there is no consensus among authors  
872 concerning the island as a whole. According to  
873 Trotet *et al.* (2001a), a continuum of top-to-ENE  
874 shearing is recorded throughout the island from  
875 the conditions of high-pressure metamorphism to  
876 those of an uneven greenschist facies overprint.  
877 A few major shear zones would have localized  
878 extensional shearing to the point that interlayered  
879 metamorphic subunits record significant differences  
880 in their pressure-temperature path (Trotet *et al.*  
881 2001b). According to Trotet *et al.* (2001a, b), the  
882 same holds for Sifnos Island. While agreeing with  
883 a continuum of extensional deformation from blues-  
884 chist to greenschist facies conditions, Bond *et al.*  
885 (2007) recently questioned the existence of these  
886 prominent shear zones on Syros and argued that  
887 extensional deformation was dominantly coaxial  
888 throughout the synmetamorphic exhumation  
889 history. Kinematic data reported by Gautier (1995)  
890 and Trotet *et al.* (2001a) do not show a dominant  
891 sense of shear on the scale of Syros Island (apart  
892 from dominantly top-to-NE/ENE shearing in the  
893 eastern part), apparently supporting the hypothesis  
894 of Bond *et al.* (2007). Finally, the southwestern  
895 chain of islands, from Kea to Sifnos, is the least  
896 known of the Cyclades (Sifnos excluded). Neverthe-  
897 less, according to Walcott & White (1998) and  
898 recent work by Grasemann *et al.* (2007), Miocene  
899 top-to-SW/SSW extensional shearing dominates  
900 on Kea, Kythnos and Serifos: these three islands  
901 are, hence, probably controlled by a major  
902 SW-dipping detachment zone. In contrast, accord-  
903 ing to Trotet *et al.* (2001a), Sifnos displays domi-  
904 nantly top-to-NE extensional shearing, hence it is  
905 probably unrelated to this detachment.

906 In the southeastern Cyclades, no domain of  
907 coaxial deformation has been found on Naxos and  
908 Paros Islands, where extensional shearing is consis-  
909 tently top-to-north (Urai *et al.* 1990; Buick 1991;  
910 Gautier *et al.* 1993). Moving toward northwestern  
911 Paros, a strong (*c.* 70°) but progressive clockwise  
912 rotation of the stretching lineation is observed  
913 (Gautier *et al.* 1993), which is thought to relate to  
914 dextral shearing along the Mid-Cycladic Lineament  
915 (Gautier & Brun 1994a). On Ikaria, almost all kin-  
916 ematic data reported by Kumerics *et al.* (2005)  
917 also indicate top-to-north shearing.

918 In contrast, the case of Ios appears more  
919 complex. Lister *et al.* (1984) initially reported mylo-  
920 nitic rocks, with top-to-south kinematic indicators,  
921 which they attributed to a ductile extensional  
922 detachment named the South Cyclades shear zone.  
923 Lister *et al.* (1984) and, more recently, Vandenberg  
924 & Lister (1996) and Forster & Lister (1999) have  
925 considered that this *c.* 200 m-thick shear zone is  
926 the main structure accommodating Neogene exten-  
927 sion on Ios. If this hypothesis is correct, then the  
928 Ios and Naxos MCCs clearly relate to two distinct

(antithetic) detachment zones. However, Gautier  
& Brun (1994a) have shown that large domains  
with top-to-north kinematic indicators are also  
found in the northern limb of Ios dome. While  
acknowledging that the sense of shear is dominantly  
top-to-south on Ios (at variance with the case on  
most islands), Gautier & Brun (1994b) favoured  
an interpretation in which the Ios MCC formed in  
the footwall of a north-dipping detachment. They  
argued that, even in this case, the Ios and Naxos  
MCCs are probably related to two distinct (though  
synthetic) detachments, because: (1) the two  
domes are well defined, so that drag folding along  
a late normal fault in between the two islands is unli-  
kely to have produced this division (especially since  
there is no evidence for such a fault in the bathyme-  
try nor in the Messinian–Quaternary sedimentary  
record; and (2) pressure conditions associated with  
greenschist facies metamorphism are similar from  
southern Naxos to Ios, and are probably even  
lower on Antiparos, an unexpected feature in the  
hypothesis of a single north-dipping detachment.  
Therefore, along a section going from Naxos to  
Ios, two distinct detachment systems are required.  
But was Ios truly dominated by non-coaxial defor-  
mation during Miocene extension, with either a  
south-dipping (Lister *et al.* 1984; Forster & Lister  
1999) or a north-dipping (Gautier & Brun 1994b)  
main detachment zone? The top-to-north kinematic  
indicators reported by Gautier & Brun (1994a) are  
associated with high-strain ductile deformation  
and are found both beneath (e.g. Gautier & Brun  
1994a, then Fig. 3b) and above the south-vergent  
South Cyclades shear zone of Lister *et al.* (1984).  
Vandenberg & Lister (1996) and Forster & Lister  
(1999) admit that top-to-north shear zones do exist  
in northern Ios, associated with mylonitic fabrics.  
Forster & Lister (1999) report these shear zones as  
cutting across the South Cyclades shear zone and  
interpret them as reflecting down-dip shearing  
along the back-tilted flank of the MCC after signifi-  
cant arching of the main shear zone (cf. Reynolds &  
Lister 1990). This interpretation is questionable,  
however, because Forster & Lister (1999) indicate  
that these crosscutting relations are observed within  
augengneiss that occupy the core of the Ios MCC,  
in which the main fabric may well relate to pre-  
extensional events (e.g. Vandenberg & Lister 1996).  
Conversely, Vandenberg & Lister (1996) suggested  
that the South Cyclades shear zone cuts across the  
north-dipping detachment zone of Naxos, yet  
acknowledging that available geochronological data  
on synkinematic intrusions do not support this scen-  
ario. Altogether, these features suggest that  
top-to-north and top-to-south extensional shear  
zones on Ios are broadly contemporaneous, and that  
there may be no dominant sense of shear on the  
scale of the island during Miocene extension.

929 Furthermore, Vandenberg & Lister (1996) and  
930 Forster & Lister (1999) mapped a series of low-  
931 angle normal faults capping the South Cyclades  
932 shear zone, associated with chloritization and breccia-  
933 tion (the Ios Detachment Fault system of Forster  
934 & Lister 1999). They consider that this fault system  
935 reflects ongoing shearing along the South Cyclades  
936 shear zone during cooling and exhumation, so that  
937 the faults are reported to have the same top-to-south  
938 kinematics. However, field evidence in favour of  
939 this interpretation is scarce. The fault system is  
940 recognized mainly in the northern limb of the  
941 dome, where the normal faults dip northward and  
942 are thus assumed to have been tilted into the attitude  
943 of apparent thrust faults during subsequent arching.  
944 However, if the top-to-north ductile shear zones also  
945 developed in response to arching, as argued by  
946 Forster & Lister (1999), then arching was already  
947 effective while the rocks were still in the conditions  
948 of ductile deformation, therefore later brittle normal  
949 fault zones could hardly have rotated through the  
950 same process. We conclude that further work is  
951 needed to check whether the 'Ios Detachment  
952 Fault system' is associated with top-to-south or  
953 top-to-north kinematics.

954 Summarizing, like the northwestern Cyclades,  
955 the southeastern Cyclades seem to include three  
956 parallel detachment systems developed during  
957 Miocene extension, coinciding with the three  
958 East–West-trending chains of islands seen at  
959 present, namely Ikaria–Samos, Paros–Naxos, and  
960 Folegandros–Ios (Gautier & Brun 1994a). The  
961 two northern chains are controlled by a north-  
962 dipping detachment zone, while the deformation  
963 pattern on Ios suggests that the southern chain has  
964 no marked asymmetry. The central chain (i.e. the  
965 islands of Naxos and Paros) displays the deepest  
966 structural levels of the Cyclades, in the form of  
967 two large domes cored with migmatites (e.g.  
968 Gautier *et al.* 1993; Jolivet *et al.* 2004).

### 970 *Interfering detachment systems*

971  
972 Using available pressure estimates for greenschist  
973 facies and locally higher temperature metamorph-  
974 ism and taking into account the present geometry  
975 and distribution of metamorphic domes in the  
976 Cyclades, Gautier & Brun (1994b) and Gautier  
977 (1995) came to the conclusion that, along at least  
978 three transects parallel to stretching (Tinos–Syros,  
979 Paros–Sikinos, Naxos–Ios), the different detach-  
980 ment zones and associated MCCs are partly super-  
981 imposed and, therefore, probably interfere with  
982 one another. They discussed two possible evolution-  
983 ary models incorporating a genetic link between  
984 successive synthetic detachment zones. A scenario  
985 was finally favoured in which a second detachment  
986 develops in the footwall of the first one, giving rise

to a secondary MCC formed in the rear flank of the  
first one (Gautier & Brun 1994b, Fig. 10). It is worth  
noting that this scenario bears some resemblance  
with the numerical simulations obtained in this  
study. Nevertheless, it has specific aspects that  
deserve a few comments. Firstly, the second detach-  
ment zone was thought to arise from prolonged  
shearing along a fault zone formed during the devel-  
opment of the first MCC (the 'Llstric Accommo-  
dation Fault' (LAF) seen in the analogue  
experiments of Brun *et al.* 1994). As a result, the  
secondary MCC was expected to show a marked  
asymmetry. It is not clear whether the present  
numerical approach is precise enough to feature a  
LAF in the brittle upper crust, therefore the mechani-  
cal background for the development of a secondary  
MCC in the simulations may be quite different;  
coincidentally, we obtain no marked asymmetry  
for the secondary MCC. Secondly, the scenario of  
Gautier & Brun (1994b) incorporated the fact that  
the two MCCs should interfere, with reference to  
the three studied transects (for this reason, the  
LAF was drawn closer to the first detachment than  
it is in the experiments of Brun *et al.* 1994).

Gautier & Brun (1994b) further pointed out that,  
with ongoing extension, this 'second footwall  
detachment' scenario may ultimately result in a  
complete omission of the wedge of upper crustal  
rocks that initially formed in the rearmost part of  
the first MCC. They claimed that this feature com-  
pares well with the situation in the Cyclades,  
where no such wedge of upper crustal rocks is  
exposed on the islands. However, the latter point  
depends on the interpretation that is made of seg-  
ments of the metamorphic pile exposing well-  
preserved eclogites and blueschists, as on Syros  
and Sifnos. Following the opinion of Avigad  
(1993) and Wijbrans *et al.* (1993) for the case of  
Sifnos, Trotet *et al.* (2001a) have proposed that  
high levels of the metamorphic pile on these two  
islands escaped pervasive retrogression because  
they were exhumed earlier. An apparent support to  
this interpretation is the fact that, on Sifnos, radio-  
metric data from these rocks provide significantly  
older ages than lower levels with intense greenschist  
facies retrogression (Altherr *et al.* 1979; Wijbrans  
*et al.* 1990). As a result, high levels of the meta-  
morphic pile may have been part of the upper  
crust by the time the rest of the pile underwent  
extensional deformation associated with greenschist  
facies metamorphism (Avigad 1993; Trotet *et al.*  
2001a; Parra *et al.* 2002). If so, the claiming of  
Gautier & Brun (1994b) that no wedge of upper  
crustal rocks exists in the Cyclades is incorrect,  
and it is not so clear whether adjacent MCCs inter-  
fere or not. For instance, much of Syros would rep-  
resent such upper crustal rocks, and the same may  
apply to Ios, where high-pressure rocks are

987 relatively abundant in the envelope of the dome,  
 988 above the South Cyclades shear zone of Lister  
 989 *et al.* (1984), displaying similarly 'old' ages as on  
 990 Syros and Sifnos (van der Maar & Jansen 1983).  
 991 Due to its potential implications, this hypothesis  
 992 needs to be further discussed.

993 According to the interpretation of Trotet *et al.*  
 994 (2001a, b), important extensional shear zones  
 995 should exist (and are reported to do so) within the  
 996 metamorphic pile of Syros and Sifnos (see also  
 997 Avigad 1993). In addition, the topmost detachment  
 998 fault seen in southeastern Syros, with Cretaceous  
 999 metamorphic rocks in the hanging wall (Maluski  
 1000 *et al.* 1987) and well preserved high-pressure  
 1001 rocks in the near footwall, should represent a rela-  
 1002 tively old structure. However, in the case of Syros,  
 1003 Bond *et al.* (2007) claim that the intermediate exten-  
 1004 sional shear zones do not exist and, like other  
 1005 authors have argued for Sifnos and Tinos Islands  
 1006 (Schliestedt & Matthews 1987; Bröcker 1990;  
 1007 Ganor *et al.* 1996), consider that the degree of pres-  
 1008 ervation of the high-pressure assemblages reflects  
 1009 primarily the extent of fluid infiltration during  
 1010 greenschist facies retrogression. Limited fluid infil-  
 1011 tration and deformation in the least retrogressed  
 1012 rocks may also account for the preservation of  
 1013 older ages by the time rocks passed through *P–T*  
 1014 conditions of the greenschist facies, as proposed  
 1015 by Wijbrans *et al.* (1990) in the case of Sifnos (see  
 1016 however Wijbrans *et al.* 1993). This is especially  
 1017 clear on Tinos, where the rocks with the best pres-  
 1018 erved high-pressure assemblages (with ages  
 1019 around 45–37 Ma) lie at the same structural level  
 1020 as those showing a complete greenschist overprint  
 1021 (with ages around 33–21 Ma; Bröcker & Franz  
 1022 1998; Parra *et al.* 2002). In this particular case, the  
 1023 extent of retrogression is apparently linked with  
 1024 the intensity of shearing during greenschist facies  
 1025 metamorphism (Jolivet & Patriat 1999; Parra *et al.*  
 1026 2002). The same may hold for Syros (Bond  
 1027 *et al.* 2007) and, eventually, Sifnos (Wijbrans  
 1028 *et al.* 1990). Rosenbaum *et al.* (2002) also consider  
 1029 that, in northern Syros, at high levels of the meta-  
 1030 morphic pile, greenschist facies overprint is local-  
 1031 ized into top-to-NE shear zones that are  
 1032 contemporaneous with Miocene extensional shear-  
 1033 ing in neighbouring islands. As for the detachment  
 1034 in southeastern Syros, its timing is poorly con-  
 1035 strained. Trotet *et al.* (2001a) used a  $^{40}\text{Ar}/^{39}\text{Ar}$   
 1036 white mica age obtained close to the contact  
 1037 ( $30.3 \pm 0.9$  Ma; Maluski *et al.* 1987) to infer that  
 1038 the detachment was active at that time. Maluski  
 1039 *et al.* (1987) reported this age from an omphacitic  
 1040 metagabbro and pointed out that the obtained spec-  
 1041 trum shows evidence for an inherited component. In  
 1042 addition, Trotet *et al.* (2001a) indicate that the  
 1043 actual detachment contact is marked by breccias  
 1044 reworking eclogites retrograded into the greenschist

facies. This strongly suggests that at least part of the  
 displacement along the detachment occurred signifi-  
 cantly later than 30 Ma, that is, at about the same  
 time as in other islands (e.g. Gautier & Brun  
 1994a). Altogether, the above features suggest  
 that, in the Cyclades as a whole, well-preserved  
 high-pressure rock assemblages represent low-  
 strain lenses of variable size embedded into a  
 single layer of greenschist facies metamorphism  
 dating from the late Oligocene–early Miocene.  
 This interpretation may apply to most islands (e.g.  
 Wijbrans *et al.* 1990; Parra *et al.* 2002; Bond *et al.*  
 2007), Ios included (Forster & Lister 1999). As a  
 result, the inference that no wedge of upper crustal  
 rocks exists in the Cyclades (Gautier & Brun  
 1994b) remains probably valid, which, in turn, sup-  
 ports the view that detachment zones and associated  
 MCCs do interfere with one another in this region. It  
 remains that, on Syros and Sifnos, an upward gradi-  
 ent of preservation of the high-pressure assemblages  
 exists across the *c.* 3 km-thick metamorphic pile  
 (e.g. Wijbrans *et al.* 1990; Trotet *et al.* 2001a).  
 We suggest that this gradient reflects the transition  
 from pervasive deformation, below, to more local-  
 ized deformation, above, within the layer of greensch-  
 ist facies metamorphism. In other words,  
 greenschist facies metamorphism in the middle  
 crust would coincide with the broad transition  
 from pervasive (ductile) to localized (ductile to  
 brittle) deformation across the thickness of the  
 crust, in good agreement with the views of Jolivet  
 & Patriat (1999) and Jolivet *et al.* (2004).

#### *Post-orogenic versus syn-orogenic extension*

The numerical simulations presented in this paper  
 are concerned with the case of whole-lithosphere  
 extension. As stated above, most authors having  
 identified extensional detachments and meta-  
 morphic core complexes in the Cyclades interpreted  
 them as resulting from Aegean 'backarc' extension  
 (Lister *et al.* 1984; Buick 1991; Gautier & Brun  
 1994b; Jolivet & Patriat 1999), thus apparently  
 fitting the experimental setup. These structures  
 developed within metamorphic rocks that  
 previously experienced high-pressure/low-  
 temperature conditions, therefore extension may  
 also be described as 'late-orogenic' (Gautier &  
 Brun 1994b). However, for the purpose of a com-  
 parison with the numerical results, it needs to be  
 discussed whether the extensional structures devel-  
 oped strictly after crustal thickening or/and during  
 ongoing thrusting beneath the locus of extension.  
 In the Aegean, these two cases have been refered  
 to as post vs. syn-thickening, or post vs. syn-  
 collisional, extension (Gautier & Brun 1994b), or  
 post vs. syn-orogenic extension/exhumation  
 (Jolivet & Patriat 1999; Trotet *et al.* 2001a; Parra

1045 *et al.* 2002; Jolivet *et al.* 2003), the latter terminol-  
1046 ogy being now widely accepted. In the following,  
1047 we prefer to use extension rather than exhumation  
1048 because exhumation may also result from erosion,  
1049 even though erosion in the Cyclades has probably  
1050 been limited during the Cenozoic (e.g. Gautier &  
1051 Brun 1994a). We emphasize that extension does  
1052 not necessarily mean that the whole lithosphere, or  
1053 even the whole crust, is stretched horizontally.  
1054 This is obvious in the case of syn-orogenic exten-  
1055 sion, where plate convergence is the leading  
1056 process and horizontal shortening the dominant  
1057 regime on the lithospheric scale. Syn-orogenic  
1058 extension is sometimes described as corresponding  
1059 to the development of an extrusion wedge (e.g.  
1060 Ring & Reischmann 2002; Ring *et al.* 2007a).

1061 The distinction between post and syn-orogenic  
1062 extension is a difficult task, especially because the  
1063 associated faults and shear zones may have the  
1064 same kinematics (Jolivet & Patriat 1999; Trotet  
1065 *et al.* 2001a). Gautier & Brun (1994b) and Gautier  
1066 *et al.* (1999) have argued that, because extension  
1067 with a direction of stretching parallel to plate con-  
1068 vergence was active at the same time (i.e. since at  
1069 least the Aquitanian) across a wide part of the  
1070 Aegean, from the Rhodope to Crete, this extension  
1071 was necessarily post-orogenic, based on a compar-  
1072 ison with the case of syn-orogenic lateral extension  
1073 in the Himalaya–Tibet orogen. However, this  
1074 assessment may be incorrect in the case of a signifi-  
1075 cant retreat of the underthrust slab during  
1076 orogeny. As discussed by Jolivet *et al.* (2003), if  
1077 the dynamics of the orogen is basically that of a  
1078 retreating subduction, then extension can be every-  
1079 where parallel to convergence, including in the  
1080 area lying above the frontal thrust zone. In a  
1081 sense, such an orogen is not strictly collisional,  
1082 therefore the description of extension as post or syn-  
1083 collisional (Gautier & Brun 1994b) is unadapted in  
1084 this case.

1085 Even if only extensional structures are observed  
1086 in a late-orogenic setting, it is usually difficult to  
1087 demonstrate that their formation was strictly post-  
1088 orogenic, because it can always be argued that  
1089 coeval thrusting possibly occurred beneath the  
1090 deepest exposed rocks. Conversely, syn-orogenic  
1091 extension is demonstrated if a thrust zone can be  
1092 shown to have been active while extension occurred,  
1093 or had already started, at shallower levels. Avigad &  
1094 Garfunkel (1989) and Avigad *et al.* (1997) tenta-  
1095 tively argued for the latter case on Tinos and Evia  
1096 islands, however their arguments have been criti-  
1097 cized by Gautier (2000) and Bröcker & Franz  
1098 (2005). Moreover, in the scenario of Avigad *et al.*  
1099 (1997) for the Cyclades, coeval thrusting and  
1100 inferred syn-orogenic extension are restricted to  
1101 the Oligocene period, while post-orogenic extension  
1102 started at about 25 Ma, associated with a pervasive

greenschist facies overprint, as in the common  
view (see above). Avigad *et al.* (1997) also  
acknowledged that the identification of structures  
associated with the period of syn-orogenic exten-  
sion is problematic.

The shape of the pressure–temperature path fol-  
lowed by metamorphic rocks may help to decipher  
between syn-orogenic and post-orogenic extension.  
Following Wijbrans *et al.* (1993), Jolivet and  
co-workers have proposed that, among the meta-  
morphic rocks of the Cyclades, those having fol-  
lowed a cold geotherm during exhumation should  
have done so owing to syn-orogenic extension  
(Jolivet & Patriat 1999; Trotet *et al.* 2001a, b;  
Parra *et al.* 2002; Jolivet *et al.* 2003). A critical ques-  
tion is how cold this geotherm should be, given that  
exhumation beneath a detachment also helps to  
prevent heating. The best answer probably comes  
from the study of Parra *et al.* (2002), showing that,  
on Tinos, rocks in the footwall of the NE-dipping  
detachment experienced an episode of isobaric  
heating (a temperature increase from 400°–550 °C  
at about 9 kbar) between two episodes of exhumation.  
Parra *et al.* (2002) convincingly proposed  
that the first and second episodes reflect syn-  
orogenic and post-orogenic extension, respectively  
(see also Jolivet *et al.* 2004). As a result, on Tinos  
at least, only post-orogenic extension would be  
recorded since rocks moved out of the conditions  
of blueschist facies metamorphism. In other  
words, all the structures developed at greenschist  
facies and subsequent lower grade conditions are  
expected to relate to post-orogenic extension, in  
agreement with earlier proposals (Gautier & Brun  
1994a; Jolivet & Patriat 1999). There does not  
seem to be a significant diachronism of greenschist  
facies metamorphism on the scale of the Cyclades  
(including at high levels of the metamorphic pile  
on Syros, see previous section), therefore the  
whole set of detachment zones and associated  
MCCs described before have probably developed  
during post-orogenic extension.

It is difficult to determine when this extension  
started. Using the data of Bröcker & Franz (1998),  
Parra *et al.* (2002) have suggested that the beginning  
of the second episode of exhumation and, therefore,  
the onset of post-orogenic extension in the Cyclades  
took place at 30 Ma (see also Jolivet *et al.* 2003,  
2004). Based on the data of Wijbrans *et al.* (1990),  
Wijbrans *et al.* (1993) have proposed a *P–T* path  
for lower levels of the metamorphic pile on Sifnos  
that resembles the one of Parra *et al.* (2002) for  
Tinos. However, in this case, isobaric heating  
(at 6.5 kbar) would have occurred from 30 Ma to  
22 Ma, so that the second episode of exhumation  
would start at 22 Ma. Nevertheless, the scenario of  
Wijbrans *et al.* (1993) assumes that post-thickening  
extension started at 30 Ma, being first confined to

1103 crustal levels beneath the presently exposed rock  
1104 pile, then migrating into this pile. Therefore, both  
1105 interpretations (Wijbrans *et al.* 1993; Parra *et al.*  
1106 2002) concur in the idea that post-orogenic exten-  
1107 sion was active in the Cyclades during the earliest  
1108 Miocene (e.g. Gautier & Brun 1994a); they even  
1109 suggest that it was already active during the late  
1110 Oligocene.

1111 In contrast, Ring and co-workers have put  
1112 forward an extreme alternative scenario, in which  
1113 a context of syn-orogenic extension would have  
1114 been maintained in the Cyclades until *c.* 21 Ma  
1115 (Ring *et al.* 2001; Ring & Reischmann 2002;  
1116 Ring & Layer 2003; Ring *et al.* 2007a). This  
1117 would have been followed by an episode of post-  
1118 orogenic extension starting later than *c.* 15 Ma  
1119 (Ring *et al.* 2007a), probably at *c.* 12 Ma (Ring &  
1120 Layer 2003), and resulting from thermal weakening  
1121 at the time the Aegean magmatic arc would have  
1122 reached the Cyclades. If this scenario is correct,  
1123 then extensional structures associated with greens-  
1124 chist facies and higher temperature metamorphism  
1125 should largely date from an episode of syn-orogenic  
1126 extension, as, for instance, on Naxos (e.g. Gautier  
1127 *et al.* 1993; Keay *et al.* 2001), Tinos (e.g. Gautier  
1128 & Brun 1994a; Bröcker & Franz 1998, 2000;  
1129 Jolivet *et al.* 2004) and Andros (Gautier & Brun  
1130 1994b; Bröcker & Franz 2006). As a result, our  
1131 attempt to compare our numerical simulations and  
1132 the Cycladic case would be questionable.

1133 According to Ring and co-workers, the Central  
1134 Aegean region is flooded by the poorly exposed  
1135 parautochthonous Basal unit, coinciding with the  
1136 Almyropotamos unit in central southern Evia (e.g.  
1137 Dubois & Bignot 1979); this unit would have been  
1138 underthrust while extensional shearing developed  
1139 at higher levels of the metamorphic pile. This  
1140 interpretation follows Avigad *et al.* (1997) except  
1141 for the timing of the episode of syn-orogenic exten-  
1142 sion (before about 25 Ma for Avigad *et al.* as late as  
1143 21 Ma for Ring and co-workers). We think that this  
1144 scenario is unlikely, especially its timing, for the  
1145 three following reasons:

1146

- 1147 • Rb–Sr and  $^{40}\text{Ar}/^{39}\text{Ar}$  dating of phengites  
1148 from samples of the Basal unit has yielded  
1149 ages mostly between 21 and 24 Ma (Ring  
1150 *et al.* 2001; Ring & Reischmann 2002; Ring &  
1151 Layer 2003). While they coincide with the  
1152 timing of greenschist facies metamorphism in  
1153 the overlying unit, these ages were interpreted  
1154 as reflecting high-pressure metamorphism in  
1155 the Basal unit (hence constraining the age of  
1156 underthrusting) because the dated phengites  
1157 have a high Si content ( $\geq 3.3$  per formula  
1158 unit). However, as thoroughly discussed by  
1159 Bröcker *et al.* (2004) and Bröcker & Franz  
1160 (2005), this interpretation is questionable and

the obtained ages are more likely to reflect  
the timing of post-high-pressure greenschist  
facies retrogression, as in the overlying unit.  
Further support to the objections of Bröcker  
*et al.* (2004) is found in the recent Rb–Sr  
study of Wegmann (2006) on rocks from south-  
easternmost Evia, at higher levels of the meta-  
morphitic pile, far above the Basal unit. In one  
rock repeatedly dated with a microsampling  
method, phengites have a Si content ranging  
from 3.36 to 3.74 pfu and yield Rb–Sr ages  
ranging from 21 to 11 Ma. Following the line  
of reasoning of Ring and co-workers, this  
would mean that higher levels of the meta-  
morphitic pile were still experiencing high-  
pressure conditions at that time. This is at  
odds with the report from the neighbouring  
northwestern Cyclades (Bröcker & Franz  
1998, 2006) and from southern Evia itself  
where, according to Ring *et al.* (2007a), such  
rocks experienced greenschist facies conditions  
as early as 21 Ma. It should also be stressed that  
the youngest fossils found so far in the Almyr-  
opotamos unit represent the lower or middle  
Eocene (Dubois & Bignot 1979), not the  
upper Eocene–Oligocene as commonly  
reported (e.g. Ring *et al.* 2007a), therefore  
this unit may have started to underthrust as  
early as during the early Eocene;

- According to the scenario of Ring and co-  
workers, the Central Aegean region should  
have been characterized by a depressed  
geotherm as late as around 21 Ma (i.e. as  
long as underthrusting and inferred high-  
pressure metamorphism were developing),  
and no significant thermal overprint is  
expected before about 14 Ma, when arc mag-  
matism is considered to have reached the  
Cyclades. However, this does not take into  
account the case of the migmatite domes on  
Naxos and Paros Islands. U–Pb dating of  
zircons from the migmatitic core of Naxos  
indicates that partial melting mostly occurred  
at *c.* 17.5 Ma and was already under way at  
20 Ma (Keay *et al.* 2001), in good agreement  
with time constraints provided by other radio-  
metric methods (e.g. Andriessen *et al.* 1979;  
Wijbrans & McDougall 1988). This shows  
that at least part of the Central Aegean  
region was actually characterized by a high  
geotherm at about 20 Ma. The Basal unit is  
unlikely to lie underneath the migmatite  
domes, because if it had been underthrust  
until 21 Ma, migmatization in the hanging  
wall of this thrust could hardly have been  
maintained until *c.* 17 Ma (cf. Keay *et al.*  
2001). Hence, the migmatite domes probably  
cut across the contact and, as stated before,

1161 represent the deepest structural levels of the  
1162 Cyclades. It is not known whether the migma-  
1163 tites seen on Naxos and Paros expand laterally  
1164 beneath the other islands, although there are  
1165 chemical data to suggest so (Gautier & Brun  
1166 1994a). Regardless, the area of Naxos and  
1167 Paros was hot at 20 Ma, and we do not  
1168 see how this can be reconciled with the  
1169 hypothesis of regional underthrusting as late  
1170 as 21 Ma; and

- 1171 Post-orogenic extension is accompanied by the  
1172 formation of grabens (as also illustrated by our  
1173 numerical experiments) which may evolve into  
1174 supra-detachment basins. Thus, the base of  
1175 the supradetachment basin stratigraphy may  
1176 provide a minimum age for the onset of post-  
1177 orogenic extension. The oldest supra-  
1178 detachment sediments known in the Cyclades,  
1179 on Naxos and Paros, are Aquitanian (23.0–  
1180 20.4 Ma; Lourens *et al.* 2004) and form the  
1181 basis of a nearly continuous stratigraphy reach-  
1182 ing the upper Miocene (Angelier *et al.* 1978;  
1183 Roesler 1978; Sanchez-Gomez *et al.* 2002).  
1184 This documents continuous formation of accom-  
1185 odation space from the Aquitanian onward,  
1186 suggesting no fundamental change in the tec-  
1187 tonic setting since that time (Gautier *et al.*  
1188 1993; Gautier & Brun 1994a; Sánchez-Gómez  
1189 *et al.* 2002). In addition, the Aquitanian and Bur-  
1190 digalian sediments are marine deposits (e.g.  
1191 Angelier *et al.* 1978), while it may be argued  
1192 that sedimentation beneath sea level is unex-  
1193 pected during (or immediately after) an episode  
1194 of extension coeval with underthrusting, as in  
1195 the scenario of Ring *et al.* co-workers.

1196 To conclude on this part, our opinion is that a  
1197 context of syn-orogenic extension could hardly  
1198 have existed in the Cyclades later than about  
1199 25 Ma, considering that at least a few million  
1200 years are necessary to enhance partial melting  
1201 after underthrusting, whatever the exact origin of  
1202 the heating event. Syn-orogenic extension finish-  
1203 ing at *c.* 37 Ma, as suggested by Parra *et al.* (2002),  
1204 would fit this condition. We also note that the  
1205 onset of post-orogenic extension at *c.* 30 Ma in the  
1206 Cyclades, as suggested by Wijbrans *et al.* (1993)  
1207 and Parra *et al.* (2002), is fully compatible with  
1208 the timing of events reported by Thomson & Ring  
1209 (2006) and Ring *et al.* (2007b) in the nearby Men-  
1210 deres massif, where the allochthonous position of  
1211 the 'blueschist' unit of the Cyclades is  
1212 well established.

#### 1213 *Did extension in the Cyclades significantly* 1214 *deviate from plane strain deformation?* 1215

1216 Finally, before comparing the Cyclades and our  
1217 numerical experiments, we should examine  
1218

whether crustal extension in the Cyclades closely  
approximated plane strain deformation, as  
assumed when extrapolating the two-dimensional  
simulations to a three-dimensional setting, or not.  
Based on the presence of folds with axes parallel  
to the mean stretching lineation on several islands  
(Naxos, Paros, Tinos and Andros), some authors  
have argued that a significant component of trans-  
verse (*c.* East–West) shortening has accompanied  
MCC-type extension in the Cyclades (Urai *et al.*  
1990; Buick 1991; Avigad *et al.* 2001; Jolivet  
*et al.* 2004). According to Avigad *et al.* (2001),  
the magnitude of this lateral contraction was high  
enough to maintain the thickness of the crust  
roughly constant despite intense extensional defor-  
mation. Transverse shortening may be viewed as a  
normal response to the three-dimensional displace-  
ment field of the Aegean lithosphere during exten-  
sional spreading (Gautier *et al.* 1999; Jolivet  
*et al.* 2004), nevertheless our opinion is that its con-  
tribution to crustal strain has never been significant  
in the Cyclades. Most of the folds taken as evidence  
for strong lateral shortening are either isoclinal  
to tight folds with low-dipping axial planes subparallel  
to the main foliation (therefore they do not properly  
document horizontal shortening) or upright open  
folds (documenting limited shortening). On Naxos,  
which is reported as the island where transverse  
shortening is best seen, Vanderhaeghe (2004) has  
shown that subvertical granitic dikes have emplaced  
throughout the inner envelope of the migmatite  
dome during extension. About one half of these  
dikes trend parallel to the *c.* North–South stretching  
lineation and another half perpendicular to it, there-  
fore bulk flattening strain and horizontal stretching  
in the East–West direction are actually documented  
(Vanderhaeghe 2004). The relatively steep attitude  
of foliations within and around the migmatitic  
core of the Naxos dome may reflect the diapiric  
ascent of the migmatites (Vanderhaeghe 2004)  
rather than folding and horizontal shortening (e.g.  
Jolivet *et al.* 2004).

In analogue experiments simulating the spread-  
ing of a weak lithosphere toward a free boundary,  
transverse shortening is present but is confined to  
the inner (northern in an Aegean frame) part of the  
deforming sheet (Gautier *et al.* 1999). The Cyclades  
are unlikely to have occupied such an inner position  
during Aegean extension, at least until the late  
Miocene, therefore the lack of clear evidence for  
significant transverse shortening in the ductile  
record of the islands is not surprising. The situation  
is possibly different since around the Pliocene (since  
<3 Ma according to Gautier *et al.* 1999, but more  
probably since <8 Ma according to the paleo-  
magnetic results of van Hinsbergen *et al.* 2005b),  
when a southward jump of the northwestern tip of  
the Aegean arc brought the Cyclades in a more

1219 inner position than they were before, and when the  
1220 westward extrusion of Anatolia started to affect  
1221 the evolution of the Aegean domain. This regional  
1222 reorganization probably explains the record of  
1223 WNW–ENE shortening (in the form of tight folds,  
1224 strike-slip and reverse faults) in Neogene sediments  
1225 of the Central Aegean region (Angelier 1977*b*),  
1226 some of which must be younger than 10 Ma  
1227 (Sánchez-Gómez *et al.* 2002).

1228 We conclude that crustal extension in the  
1229 Cyclades probably coincided with near-plane  
1230 strain deformation during much of the period of  
1231 post-orogenic extension (i.e. except possibly  
1232 since < 8 Ma), therefore comparing the evolution  
1233 of the Cyclades with our two-dimensional exper-  
1234 iments bears some logic.

## 1237 Comparison and discussion

### 1238 *Comparison between the numerical* 1239 *experiments and the Cyclades*

1240 The previous overview has shown that several  
1241 aspects of the tectonic evolution of the Cyclades  
1242 during the Neogene are reminiscent of the results  
1243 of our numerical experiments, especially the coexis-  
1244 tence of several MCCs and associated detachment  
1245 systems along a section parallel to extension  
1246 ('How many MCC and detachment systems in the  
1247 Cyclades?' section) and the fact that at least some  
1248 of these MCCs interfere with one another ('Interfer-  
1249 ing detachment systems' section). In addition, we  
1250 have shown that the general kinematic framework  
1251 that prevailed during the development of these  
1252 structures is comparable to the one in our exper-  
1253 imental setup, that is, a context of whole-lithosphere  
1254 (i.e. post-orogenic) extension ('Post-orogenic vs.  
1255 syn-orogenic extension' section) associated with  
1256 near-plane strain deformation (precious section).  
1257 We now compare in more detail the results of our  
1258 numerical experiments with the geological record  
1259 of the Cyclades. Four essential issues are compared:  
1260 the final depth of the Moho, the geometry of MCCs,  
1261 their kinematic pattern, and the amount of time  
1262 associated with their exhumation:

1263 *Moho depth.* In the experiments, the Moho interface  
1264 remains nearly flat throughout the extensional  
1265 process (Fig. 5). The final Moho depth increases  
1266 with increasing initial crustal thickness and with  
1267 decreasing boundary velocity (Fig. 7). Within the  
1268 range of conditions giving rise to interfering  
1269 MCCs (see 'Numerical experiments' section), this  
1270 depth varies between 22.5 and 29 km. In the  
1271 Cyclades, various geophysical investigations indi-  
1272 cate that the Moho is almost flat, lying at depths  
1273 around 25–26 km (Makris & Veis 1977; Makris

1978; Vigner 2002; Li *et al.* 2003; Tirel *et al.*  
2004*b*), well within the expected range of values.  
According to the experiments, a value of 25–  
26 km is compatible with an initial crustal thickness  
(at the onset of post-orogenic extension) of *c.* 43–  
44 km (Fig. 7*e*) and a boundary velocity of *c.* 2.0–  
2.3 cm/a (Fig. 7*f*).

*Geometry of MCCs.* Before comparing the geometry  
(this section) and kinematic pattern (next section) of  
MCCs in the numerical simulations and in the  
Cyclades, it must be stressed that, unlike in the  
experimental setup, the crust of the Cyclades was  
neither homogeneous nor isotropic at the onset of  
post-orogenic extension. Most authors agree on  
the view that crustal thickening during the earlier  
orogenic period occurred through the operation of  
dominantly SSW-vergent thrusts (e.g. Bonneau  
1982; Jolivet *et al.* 2003; van Hinsbergen *et al.*  
2005*a*). It may be suspected that some of these  
thrusts were later reactivated as normal-sense  
detachment zones (e.g. Gautier *et al.* 1993; Avigad  
*et al.* 1997; Trotet *et al.* 2001*a*; Jolivet *et al.* 2003;  
Ring *et al.* 2007*a*), which may account for the pre-  
dominance of top-to-NNE shearing during exten-  
sion on the scale of the Cyclades. However, clear  
evidence that earlier thrusts have particularly loca-  
lized later extensional shearing is missing. On Ios  
Island, Vandenberg & Lister (1996) suggested that  
the south-vergent South Cyclades shear zone  
partly reactivates (in extension) a north-vergent  
Alpine thrust, however the arguments for such a  
thrust are unclear. It remains that dominantly  
SSW-vergent Alpine thrusting has certainly pro-  
duced a broadly north-dipping stack of various  
lithologies, the weakest of which may have loca-  
lized later extensional shearing. Thus, not only the  
predominance of top-to-NNE shearing during  
extension might be explained by earlier thrusting,  
so does the spatial distribution of extensional  
detachments, which could in part reflect the initial  
geometry of the thrust stack. We are aware of this  
problem when comparing the Cyclades with the  
numerical simulations, the problem arising from  
our deliberate choice of the simplest possible  
initial conditions in the experimental setup.

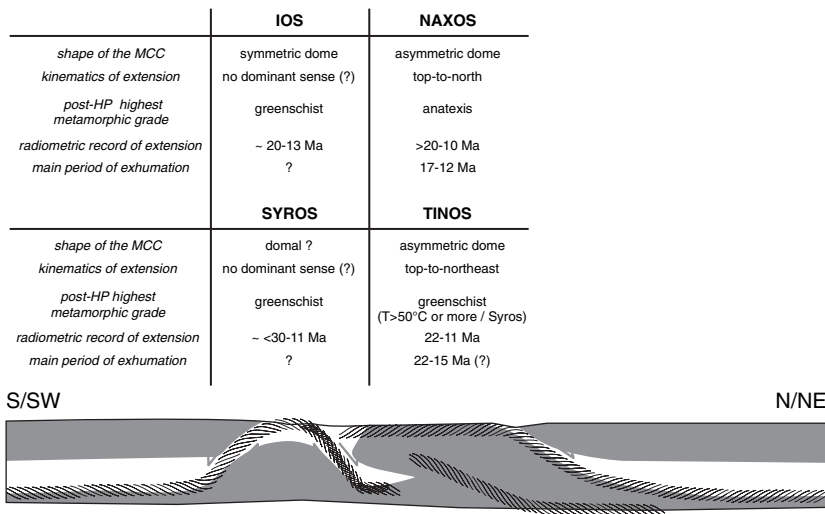
Nevertheless, as the simulations compare rela-  
tively well with the natural case, our impression is  
that the role of pre-existing structures has been  
minor during post-orogenic extension in the  
Cyclades. We suspect that this arises from the  
high thermal profile of the crust at, or soon after,  
the initiation of post-orogenic extension. Accord-  
ing to our experiments, at least the lower half of  
the crust was at temperatures in excess of 550 °C,  
at which the viscosity contrast between the most  
common rock types is severely reduced. At these  
levels, the most significant viscosity drops relate

1277 to the progress of anatexis, which depends only  
1278 partly on the geometry of earlier thrusting.

1279 A number of observations imply that several  
1280 MCCs coexist in the Cyclades (see ‘How many  
1281 MCC...’ section). Structural data suggest that  
1282 three detachment systems and associated MCCs  
1283 have developed in both the northwestern Cyclades  
1284 (coinciding with the Evia–Mykonos, Gyros–  
1285 Syros and Kea–Sifnos island chains) and the  
1286 southeastern Cyclades (coinciding with the  
1287 Ikaria–Samos, Paros–Naxos and Folegandros–Ios  
1288 island chains). As discussed by Gautier & Brun  
1289 (1994*b*), the MCCs of at least two of these chains  
1290 apparently interfere with one another, based on the  
1291 relationships between Naxos and Ios, Paros and  
1292 Sikinos, and Tinos and Syros (see ‘Interfering  
1293 detachment systems’ section). We now focus on a  
1294 comparison between the numerical simulations  
1295 and the Naxos–Ios and Tinos–Syros island pairs,  
1296 leaving Paros–Sikinos aside because it repeats the  
1297 case of Naxos–Ios without an equivalent structural  
1298 or geochronological dataset being available.

1299 We find striking similarities between the simu-  
1300 lations and the selected island pairs in terms of geo-  
1301 metry (Fig. 9). Naxos constitutes a large MCC with a  
1302 pronounced asymmetry, exhuming high-temperature  
1303 lower crustal rocks (e.g. Gautier *et al.* 1993). Ios  
1304 constitutes another MCC (e.g. Vandenberg &  
1305 Lister 1996) formed in the direction opposite to  
1306 the slope of the Naxos detachment. The Ios dome  
1307 seems symmetric (at least, its asymmetry is not as  
1308 pronounced as on Naxos or Paros). It is apparently  
1309 narrower than the Naxos dome (although both are

partly hidden beneath sea level) and exposes lower  
grade rocks (e.g. van der Maar & Jansen 1983), indi-  
cating that the Ios MCC is less developed. The Ios  
dome is superimposed on the southern flank of the  
Naxos dome (Gautier & Brun 1994*b*). Although  
less clearly expressed, the Tinos–Syros island pair  
displays a similar geometry. Tinos is an asymmetric  
MCC exhuming rocks with a pervasive greenschist  
facies overprint (Gautier & Brun 1994*a*; Jolivet &  
Patriat 1999; Parra *et al.* 2002). Syros is another  
MCC formed in the direction opposite to the slope  
of the Tinos detachment. However, Syros does not  
show a regular dome, which may be due to the mod-  
erate size of the island and to the influence of large  
normal faults cutting across the metamorphic series  
(Ridley 1984). It exposes rocks with broadly a less  
intense greenschist facies overprint than on Tinos  
(e.g. Trotet *et al.* 2001*a*). We have discussed in  
the ‘Interfering detachment systems’ section the  
possible interpretations of this feature, suggesting  
that the upward gradient of preservation of the high-  
pressure assemblages across the metamorphic pile  
of Syros (and Sifnos) may reflect the transition  
from pervasive deformation, below, to more local-  
ized deformation, above, within a coherent layer  
of greenschist facies metamorphism. If so, then at  
least part of Syros exposes rocks of slightly shall-  
ower origin than on Tinos. This hypothesis is sup-  
ported by a comparison of the *P–T* paths of the  
deepest rocks on Syros (Trotet *et al.* 2001*b*) and  
Tinos (Parra *et al.* 2002), showing that, along the  
greenschist facies segment of the exhumation path,  
temperatures were  $\geq 50^\circ$  higher in the case of



1312  
1313  
1314  
1315  
1316  
1317  
1318  
1319  
1320  
1321  
1322  
1323  
1324  
1325  
1326  
1327  
1328  
1329  
1330  
1331  
1332 **Fig. 9.** Comparison between a crustal-scale cross-section showing interfering MCCs, as deduced from the numerical  
1333 analysis, and relevant data from two transects in the Cyclades showing closely spaced MCCs, as discussed in the  
1334 text. The comparison reveals a good agreement.

Tinos. In our experiments, the isotherms are carried upward during the earlier stages of MCC development, therefore we expect a rock of deeper origin to experience higher temperatures during exhumation, as also clearly illustrated by the numerical experiments of Gessner *et al.* (2007). Thus, the Tinos MCC has apparently accommodated more exhumation than the Syros MCC has. Note that the same process of upward heat transport during MCC development might also account for the different  $P$ – $T$  paths obtained by Trotet *et al.* (2001*b*) across the metamorphic pile of Syros and Sifnos (see e.g. Gessner *et al.* 2007, Fig. 6). As discussed by Gautier & Brun (1994*b*), the Syros MCC is probably superimposed on the southwestern flank of the Tinos MCC.

Summing up, the geometry of MCCs along the Naxos–Ios transect and, to a less extent, the Tinos–Syros transect, compares well with the numerical simulations (Fig. 9). The comparison is more convincing with type 2 experiment, in which the second dome develops in the immediate vicinity of the first dome, so that the two MCCs are partly superimposed (Figs 5*d*, *e*, *f* and 6). In this case, no wedge of upper crustal rock is preserved between the MCCs, a feature that Gautier & Brun (1994*b*) have claimed to characterize the Cyclades. If, alternatively, higher levels of the metamorphic pile on Syros (and Sifnos) represent rocks that were exhumed to upper crustal conditions before the onset of post-orogenic extension (e.g. Trotet *et al.* 2001*a*; see discussion in ‘Interfering detachment systems’ section), then the structure is broadly the same, with only the Syros MCC being less developed (i.e., leaving a cap of upper crustal rocks near the apex of the dome).

In addition, special attention should be paid to the width of the two largest MCCs of the Cyclades, on Naxos and Paros. According to the above comparison, these two domes represent MCCs of the first generation. In the experiments, depending on the initial conditions, the width of the first dome is quite variable (Fig. 7*a*, *b*). The width of Naxos and Paros domes, measured in the same way as in the experiments (from the front of the detachment, plunging northward, to the rearmost part of the dome, before reaching a wedge of brittle upper crust) is at least 35 km and most probably less than 60 km. This range is compatible with an initial crustal thickness between *c.* 41 and 44 km, and seems to exclude greater values (Fig. 7*a*). It also seems to exclude a boundary velocity lower than *c.* 2 cm/a (Fig. 7*b*). Thus, the width of the MCCs of the first generation suggests broadly the same range of initial conditions as the final Moho depth does (see ‘Moho depth’ section).

*Kinematic pattern.* Similarities are also found between the simulations and the Naxos–Ios and Tinos–Syros island pairs in terms of kinematic development of the MCCs. However, before attempting a comparison, we should keep in mind the origin of shear zones in the numerical experiments, and address the question whether the same process could have operated in the Cyclades. In the experiments, faulting occurs in the upper crust due to the imposed horizontal stretching; a major fault (i.e., a detachment) ultimately develops at this level if stretching is strong enough (see ‘Description of two experiments’ section; see also Tirel *et al.* 2004*a*). In the lower crust, ductile shear zones develop as a by-product of the process of inward flow. In the Cyclades, Gautier and Brun (1994*a*, *b*) have interpreted the shear zone pattern of some of the islands (especially Tinos, Andros, Ios) as reflecting such a process of inward flow (see ‘How many MCC...’ section). On Tinos and Andros, there is good evidence that this shear zone pattern developed during greenschist facies metamorphism and subsequent cooling to conditions corresponding to the transition from pervasive ductile to localized semi-brittle behaviour (Gautier & Brun 1994*a*; Gautier 1995; Jolivet & Patriat 1999; Jolivet *et al.* 2004; Mehl *et al.* 2005). In our experiments, shearing due to inward flow occurs significantly below the ductile–brittle transition (i.e., at temperatures at least *c.* 150 °C higher than the temperature of *c.* 300 °C obtained for the transition), nevertheless it is conceivable that shearing may propagate up to this interface if the ductile–brittle transition is to become a low-strength horizon after a certain amount of crustal extension is achieved (see ‘How many MCC...’ section). The structural record on Tinos and Andros shows that this situation may hold in the Cyclades. In addition, as micaschists and marbles dominate among the various rock types found in the islands, shearing due to inward flow may propagate at even shallower depths (that is, along an isotherm of less than 300 °C) if the proper rheological laws were used, instead of that of quartz-diorite. Nevertheless, orthogneisses apparently dominate at lower levels of the Cyclades rock pile, as seen on Naxos, Paros and Ios (e.g. van der Maar & Jansen 1983; Gautier *et al.* 1993), therefore the choice of quartz diorite as the representative rock type for the Central Aegean crust as a whole seems justified (see also Jolivet *et al.* 2003, 2004).

As mentioned before, Naxos and Paros Islands are asymmetric domes that consistently display top-to-north shear criteria. These kinematics are observed from the envelope of the domes (Gautier *et al.* 1993) down to the migmatitic core of Naxos (Buick 1991) and the poorly defined migmatitic domain of Paros (Gautier *et al.* 1993). Hence, in

1393 the Cyclades, the largest MCCs, associated with the  
1394 most pronounced exhumation, do not display evi-  
1395 dence of inward flow emanating from the rear part  
1396 of the dome (that is, inward flow that would  
1397 produce shearing antithetic to the main detachment  
1398 zone) whereas, according to the interpretation of  
1399 Gautier & Brun (1994*a, b*), less mature MCCs do  
1400 so. This may be viewed as a paradox, however,  
1401 the present experiments show that it is not. As  
1402 seen on Figure 5, SZ1, which relates to this anti-  
1403 thetic inward flow toward the main dome, is pro-  
1404 nounced but confined to great depths and, unlike  
1405 SZ2, never reaches the surface. In contrast, in the  
1406 case of the secondary dome, the two limbs coincide  
1407 with antithetic shear zones that extend upward the  
1408 two flat-lying shear zones (SZ11 and SZ12) devel-  
1409 oped in response to renewed inward flow. As a con-  
1410 sequence, the secondary dome tends to be  
1411 symmetric, and it can be expected that no dominant  
1412 sense of shear will be found around its apex. These  
1413 features compare relatively well with the case of Ios  
1414 and Syros Islands (see 'How many MCC...' section).  
1415 As mentioned in 'Analysis of the two  
1416 experiments' section, SZ12 reactivates SZ1 in oppo-  
1417 site sense but with less strain accumulated, therefore  
1418 it can be expected that relics of the first kinematics  
1419 will be found along SZ12. While assuming that  
1420 the Ios MCC was controlled by a north-dipping  
1421 detachment, Gautier & Brun (1994*b*) suggested  
1422 that this feature may explain the predominance of  
1423 top-to-south shearing across the Ios dome (that is,  
1424 top-to-south shearing would in part reflect early  
1425 inward flow in the rear flank of the Naxos MCC).  
1426 However, because the relations between  
1427 top-to-south and top-to-north shearing are unclear  
1428 on Ios (see 'How many MCC...' section), we  
1429 leave it open whether this hypothesis makes sense.  
1430 The same applies to Syros, which is possibly domi-  
1431 nated by coaxial deformation, but where there is no  
1432 indication of an early top-to-SW shearing event that  
1433 would be overprinted by top-to-NE shearing (e.g.  
1434 Trotet *et al.* 2001*a*; see 'How many MCC...' section).

1436 Summarizing, both the geometry (cf. previous  
1437 section) and the kinematic pattern of MCCs  
1438 compare well between the experiments and the  
1439 Naxos–Ios and Tinos–Syros island pairs (Fig. 9).  
1440 In both cases, the comparison holds for two  
1441 among three chains of islands, and, thus, seems to  
1442 ignore the Ikaria–Samos and Kea–Sifnos chains.  
1443 It should be reminded that, in the experiments  
1444 with interfering MCCs, additional MCCs do  
1445 develop (see 'Description of two experiments'  
1446 section), located at far distance from the MCCs  
1447 under discussion, so that the former do not interfere  
1448 with the latter (i.e. they are not superimposed nor  
1449 they rework earlier shear zones). We tentatively  
1450 suggest that the Ikaria–Samos and Kea–Sifnos

chains, which lie relatively far from the other  
chains, coincide with these non-interfering MCCs.

*Timing of exhumation.* The simulations and the  
Cyclades are now compared in terms of chronology  
using two approaches. Firstly, the comparison may  
concern the total time elapsed from the onset of  
post-orogenic extension until the time the develop-  
ment of all MCCs has reached an end. The latter  
bound is not equivalent to the end of the extensional  
process because lithospheric stretching may persist  
due to unchanged boundary conditions. However,  
due to crustal thinning, the style of extension is  
expected to change, and the development of  
MCCs to be arrested (e.g. Buck 1991), which is  
indeed what we observe in the experiments (see  
also Tirel *et al.* 2008). The amount of time defined  
in this way is here termed the duration of  
MCC-type extension. In the experiments, within  
the range of conditions giving rise to interfering  
MCCs, the duration of MCC-type extension varies  
between 16 and 32 Ma (Fig. 7). In the Cyclades,  
it can be estimated as follows: for the onset of post-  
orogenic extension, following the discussion in  
'Post-orogenic vs. syn-orogenic extension' section,  
we take 30 Ma (e.g. Parra *et al.* 2002; Jolivet *et al.*  
2004) as the earliest possible date, which is consist-  
ent with the record in the nearby Menderes massif  
(Thomson & Ring 2006; Ring *et al.* 2007*b*). The  
latest possible date is *c.* 23 Ma (Gautier & Brun  
1994*a*; Bröcker & Franz 1998, 2005, 2006). As for  
the end of MCC-type extension, a change in struc-  
tural style seems indeed recorded in the Cyclades  
during the late Miocene, when regional-scale high-  
angle faulting, bounding Messinian–Quaternary  
basins, succeeded to fast cooling of the meta-  
morphic domes, vanishing in the time range *c.*  
11–6 Ma (Gautier & Brun 1994*a*; Sánchez-Gómez  
*et al.* 2002; Hejl *et al.* 2002, 2003; Kumerics *et al.*  
2005; Iglseider *et al.* 2006; Brichau *et al.* 2006,  
2007). This is in line with the Messinian age for  
the oldest sediments nonconformably covering the  
metamorphic series on Milos (van Hinsbergen  
*et al.* 2004). We thus set the end of MCC-type exten-  
sion in between 11 and 6 Ma. It is worth noting that  
the youngest evidence of fast cooling in the footwall  
of a low-dipping detachment is provided by islands  
largely made up of a young I-type intrusion, like  
Ikaria, Serifos, Mykonos and the western part of  
Naxos (Altherr *et al.* 1982; Hejl *et al.* 2002, 2003;  
Kumerics *et al.* 2005; Iglseider *et al.* 2006; Brichau  
*et al.* 2006). It is therefore possible that arc magma-  
tism locally had the capacity of delaying the end of  
MCC-type extension by a few million years, although  
Brichau *et al.* (2006) argue that, on Naxos, the intrusion  
of the *c.* 12 Ma-old granodiorite had a negligible effect  
on the kinetics of the detachment system. Combining  
the above dates, the

1451 duration of MCC-type extension in the Cyclades is  
 1452 between 12 and 24 Ma, in good agreement with  
 1453 the experimental range. It is compatible with any  
 1454 initial crustal thickness in the range of 40–50 km  
 1455 (Fig. 7c) while it seems to exclude a boundary velocity  
 1456 lower than *c.* 1.7 cm/a (Fig. 7d).

1457 Secondly, the comparison may concern the relative  
 1458 timing of MCC development along a section  
 1459 parallel to stretching, as in the case of the Naxos–  
 1460 Ios and Tinos–Syros island pairs. In the exper-  
 1461 iments (and in the scenario favoured by Gautier &  
 1462 Brun 1994b), the second dome starts to develop  
 1463 once the first dome has achieved much of its exhu-  
 1464 mation (Fig. 5). This suggests that the period of  
 1465 fastest cooling in the first dome should predate  
 1466 that in the second dome. For instance, in  
 1467 Figure 5a, the first dome experiences fast cooling  
 1468 between the time slices 7.0 Ma and 11.4 Ma, while  
 1469 the second dome does so later, until about  
 1470 17.4 Ma. At first sight, this relation seems to imply  
 1471 that cooling ages should be older in the first dome.  
 1472 However, this is not necessarily correct, because  
 1473 the amount of exhumation is also different  
 1474 between the two domes. In Figure 5a, at 7.0 Ma,  
 1475 the green layer is approximately bounded by the iso-  
 1476 therms 350 and 550 °C, therefore it represents rocks  
 1477 in greenschist facies conditions. Rb–Sr white mica  
 1478 ages from this layer would normally date this  
 1479 stage at 7.0 Ma. Considering the range of estimates  
 1480 for the closure temperature of argon in white mica,  
 1481 between about 330 and 450 °C (e.g. Wijbrans &  
 1482 McDougall 1988; Kirschner *et al.* 1996),  
 1483 <sup>40</sup>Ar/<sup>39</sup>Ar white mica ages from this layer should  
 1484 also broadly date the stage at 7 Ma, or possibly the  
 1485 stage at 11.4 Ma, when at least the upper half of  
 1486 the green layer lies above the 350 °C isotherm. In  
 1487 the first dome, the greenschist facies layer, together  
 1488 with deeper rocks, are fastly exhumed within the  
 1489 same time range, from 7.0 to 11.4 Ma. The same  
 1490 relations are observed in Type 2 experiment. At  
 1491 the end of MCC-type extension, especially in  
 1492 Type 2 experiment (Fig. 5d), the second dome  
 1493 exposes only rocks of the greenschist facies layer,  
 1494 therefore white mica ages from this dome are  
 1495 expected to be not significantly different from  
 1496 white mica ages and higher temperature chro-  
 1497 nometers (e.g. U–Pb on zircon, <sup>40</sup>Ar/<sup>39</sup>Ar on horn-  
 1498 blende) from the first dome (e.g. in Fig. 5, within  
 1499 the time range from 7.0 to 11.4 Ma, i.e. within ≤4.4  
 1500 Ma). Moreover, Figure 5b shows that, at the same  
 1501 time the second dome rises, shearing is still active  
 1502 along the frontal detachment of the first dome (cf.  
 1503 the stage 17.4 Ma). Hence, cooling ages from this  
 1504 frontal segment of the first dome are expected to  
 1505 be as young as the cooling ages of the second  
 1506 dome. Altogether, these relations suggest that  
 1507 there is not necessarily a significant difference to  
 1508 be expected in the geochronological record of the

two domes. The only marked difference should  
 concern the period of fastest cooling, however it is  
 possible that the second dome does not raise  
 enough to allow a proper documentation of this  
 fast cooling period on geochronological grounds.

On Naxos, a period of fast cooling is recorded in  
 the migmatitic core and amphibolite facies inner  
 envelope of the dome in between ca. 16 and 8 Ma  
 (Wijbrans & McDougall 1988; Gautier *et al.*  
 1993), following an anatectic event that lasted  
 from at least 20 Ma until *c.* 17 Ma (Keay *et al.*  
 2001). The period of fastest exhumation probably  
 occurred between the end of the anatectic event  
 and the emplacement of the Western Naxos Gran-  
 odiorite (Gautier *et al.* 1993), that is, between about  
 17 and 12 Ma according to the data of Keay *et al.*  
 (2001). S-type granites emplaced in the inner enve-  
 lope of the dome at 15.5–12 Ma (Keay *et al.* 2001),  
 possibly as a result of decompression melting at  
 deeper levels of the rock pile during fast exhu-  
 mation. Ongoing core complex development after  
 12 Ma is indicated by the syn-kinematic character  
 of the Western Naxos Granodiorite with respect to  
 the north-dipping detachment zone, and by the sub-  
 sequent development of massive cataclasites along  
 the contact between the two (Urai *et al.* 1990;  
 Buick 1991; Gautier *et al.* 1993). A pseudotachylite  
 vein from this contact is dated at 10 Ma (Andriessen  
*et al.* 1979). According to Brichau *et al.* (2006),  
 brittle shearing along the detachment occurred as  
 late as 8.2 ± 1.2 Ma, based on low-temperature  
 thermochronology. As mentioned above, the intru-  
 sion of a large amount of arc-related magma (i.e.  
 the Western Naxos Granodiorite) may have sus-  
 tained the development of the Naxos MCC for a  
 longer time, although this is not the hypothesis  
 favoured by Brichau *et al.* (2006). As a fact, the  
 two youngest ages obtained by Brichau *et al.*  
 (2006) come from the northern part of the meta-  
 morphic dome, seemingly far from the granodiorite.  
 This area also yields the youngest K–Ar and  
<sup>40</sup>Ar/<sup>39</sup>Ar hornblende and biotite ages from the  
 dome (Andriessen *et al.* 1979; Wijbrans &  
 McDougall 1988), a feature that it is tempting to  
 attribute to progressive northward migration of  
 unroofing in the footwall of the detachment  
 (Gautier *et al.* 1993; Brichau *et al.* 2006).  
 However, this could also result from the emplace-  
 ment of the Western Naxos Granodiorite or an  
 equivalent young intrusion beneath this area, as pro-  
 posed by Andriessen *et al.* (1979), Wijbrans &  
 McDougall (1988) and Keay *et al.* (2001). Such an  
 intrusion actually exists, as indicated by the local  
 occurrence in northernmost Naxos of a hornblende-  
 bearing I-type granite dated at *c.* 12 Ma (Keay *et al.*  
 2001). Hence, it is possible that ongoing develop-  
 ment of the Naxos MCC after 12 Ma has occurred  
 owing to the emplacement of arc-related magmas.

1509 In the rear part of the dome, rocks that did not  
1510 experience temperatures higher than 550 °C were  
1511 at about 500 °C at *c.* 22.5–20 Ma and cooled to  
1512 about 300 °C at *c.* 14–11 Ma (Andriessen *et al.*  
1513 1979; Wijbrans & McDougall 1988; Andriessen  
1514 1991).

1515 The cooling history of the Ios MCC is not well con-  
1516 strained. A  $^{40}\text{Ar}/^{39}\text{Ar}$  white mica pseudo-plateau age  
1517 at about 20.5 Ma is considered to date shearing along  
1518 the South Cyclades shear zone (Baldwin & Lister  
1519 1998). A Rb–Sr white mica age from a deformed  
1520 aplitic vein at  $13.2 \pm 0.4$  Ma (Henjes-Kunst &  
1521 Kreuzer 1982) together with  $^{40}\text{Ar}/^{39}\text{Ar}$  potassium  
1522 feldspar minimum apparent ages at about 14 Ma  
1523 from mylonitic augengneiss (Baldwin & Lister 1998)  
1524 date another (distinct?) shearing event (vandenber-  
1525 g & Lister 1996; Baldwin & Lister 1998). This  
1526 second event is suspected to reflect the influence of  
1527 the mid-Miocene magmatism of the Cyclades, yet,  
1528 so far, there is no clear evidence for any Miocene  
1529 intrusion on Ios. Hence, the ages at 13–14 Ma may  
1530 relate to deformation without a specific thermal  
1531 event. Apatite fission track ages indicate cooling  
1532 below about 100 °C between  $13.3 \pm 1.1$  and  
1533  $8.3 \pm 1.1$  Ma (Hejl *et al.* 2003). Comparing the geo-  
1534 chronological record on Naxos and Ios, we find no  
1535 significant diachronism. As explained above,  
1536 because the Ios MCC is associated with much less  
1537 exhumation, this observation is not incompatible  
1538 with the Ios dome having formed later.

1539 On Tinos,  $^{40}\text{Ar}/^{39}\text{Ar}$  and Rb–Sr ages on white  
1540 mica indicate that greenschist facies top-to-NE  
1541 extensional shearing occurred at about 24–21 Ma  
1542 (Bröcker & Franz 1998, 2005). The detachment  
1543 zone is crosscut by the Tinos composite intrusion  
1544 and associated thermal aureole (Altherr *et al.*  
1545 1982; Avigad & Garfunkel 1989; Bröcker & Franz  
1546 2000). Rb–Sr and K–Ar ages from the main  
1547 I-type granite (Altherr *et al.* 1982; Avigad *et al.*  
1548 1998) and its thermal aureole (Bröcker & Franz  
1549 2000) suggest an early cooling at 15.5–14 Ma.  
1550 Whole-rock Rb–Sr dating indicates that marginal  
1551 S-type intrusions emplaced at the same time  
1552 (Altherr *et al.* 1982; Bröcker & Franz 1998).  
1553 Altherr *et al.* (1982) originally argued that the  
1554 main granite probably emplaced before 17 Ma,  
1555 however available radiometric data are compatible  
1556 with the view that it did so at around 15 Ma (see dis-  
1557 cussion in Bröcker & Franz 2000). Recent U–Pb  
1558 dating of zircons from the main intrusion has  
1559 yielded an age of  $14.6 \pm 0.2$  Ma (Brichau *et al.*  
1560 2007), supporting the latter view. On the one  
1561 hand, this indicates that much of the displacement  
1562 along the detachment zone occurred before 15 Ma.  
1563 On the other hand, the margins of the plutonic  
1564 complex show evidence of top-to-NE shearing  
1565 during and subsequent to emplacement (Gautier &  
1566 Brun 1994a; Bröcker & Franz 1998; Jolivet &

Patriat 1999; Brichau *et al.* 2007). A series of sub-  
vertical NW–SE-trending dykes dated at 12–  
11 Ma (Avigad *et al.* 1998) documents ongoing  
NE–SW stretching once the rocks reached the  
brittle upper crust (see also Mehl *et al.* 2005).  
Final cooling at around 12–9 Ma is documented  
by apatite fission track ages from the main intrusion  
(Altherr *et al.* 1982; Hejl *et al.* 2002; Brichau *et al.*  
2007). It is difficult to establish whether, and when,  
a period of fastest exhumation occurred on Tinos,  
especially because it is not clear where the ages of  
24–21 Ma should be plotted along the greenschist  
facies segment of the pressure–temperature path.  
If, however, a closure temperature of about 500 °C  
is accepted for the Rb–Sr system in white mica  
(Bröcker & Franz 1998, 2005), then, using the  
path obtained by Parra *et al.* (2002), this age range  
should coincide with pressures around 6 kbar. Press-  
ures associated with the thermal aureole of the *c.* 15  
Ma-old Tinos intrusion are around 2–3 kbars (e.g.  
Bröcker & Franz 2000). Taken together, using a  
factor of 3.64 to convert pressures (kbar) into  
depths (km), these values yield a mean exhumation  
rate around 1.5–2 mm/a during the period from  
*c.* 22 to 15 Ma. The apatite fission track ages indi-  
cate that later exhumation was slower. If the  
earlier episode of heating at about 9 kbar ended at  
*c.* 30 Ma, as suggested by Parra *et al.* (2002) (see  
'Post-orogenic versus syn-orogenic extension'  
section), then a mean exhumation rate around  
1.4 mm/a is suggested for the period from *c.* 30 to  
22 Ma. These estimates are crude, nevertheless  
they suggest that exhumation proceeded either at  
constant rate from *c.* 30 Ma to 15 Ma, or was a bit  
faster during the 22–15 Ma interval.

The cooling history of Syros is very poorly  
known. At least part of the displacement along the  
detachment seen in southeastern Syros occurred  
later than 30 Ma (see 'Interfering detachment  
systems' section). Zircon fission track ages are  
around 20 Ma in the hanging wall and around  
11 Ma in the footwall, suggesting that the detach-  
ment was active at *c.* 11 Ma (Ring *et al.* 2003).  
All the footwall samples come from northern  
Syros, so that it is not clear whether the age gap of  
9 Ma reflects displacement along the detachment  
itself or/and along one of the low-angle normal  
faults that dissect the footwall (Ridley 1984).  
Summing up, a sound comparison between Tinos  
and Syros is out of reach so far, nevertheless avail-  
able radiometric data leave it possible that the Tinos  
MCC formed earlier.

The above review also indicates that the two island  
pairs (Naxos–Ios and Tinos–Syros) may have  
formed contemporaneously. The Naxos MCC experi-  
enced its fastest exhumation between *c.* 17 and 12 Ma,  
while the Tinos MCC may have done so between *c.* 22  
and 15 Ma. Thus, the two MCCs could be broadly

1567 coeval. In contrast, Jolivet *et al.* (2004) claimed that  
 1568 the Naxos MCC has formed *c.* 5 Ma later than the  
 1569 Tinos MCC has. They further proposed that, in the  
 1570 Cyclades, ‘a-type’ MCCs (domes with an axis parallel  
 1571 to extension, like on Naxos) are associated with  
 1572 greater exhumation and formed later than ‘b-type’  
 1573 MCCs (domes with an axis perpendicular to extension,  
 1574 like on Tinos). This interpretation largely  
 1575 arises from the assumption that the main intrusion  
 1576 on Tinos emplaced as early as 20–19 Ma, as initially  
 1577 proposed by Altherr *et al.* (1982). As stated above,  
 1578 however, available radiometric data make it possible  
 1579 that the whole composite intrusion of Tinos emplaced  
 1580 at *c.* 15 Ma. We also notice that the Ios MCC is  
 1581 clearly a ‘a-type’ dome (e.g. Gautier & Brun 1994a;  
 1582 Vandenberg & Lister 1996), yet, at variance with  
 1583 the hypothesis of Jolivet *et al.* (2004), it did not  
 1584 exhume higher grade rocks than the Tinos MCC  
 1585 did, and recorded extensional shearing as early as  
 1586 *c.* 20.5 Ma (Baldwin & Lister 1998), that is, at the  
 1587 same time as on Tinos.

#### 1589 *Implications for the conditions of extension* 1590 *in the Cyclades* 1591

1592 Insofar as the numerical experiments presented in  
 1593 this study adequately simulate the process of litho-  
 1594 spheric extension, their comparison with the case  
 1595 of the Cyclades suggests a relatively narrow range  
 1596 of conditions for the development of post-orogenic  
 1597 extension in the Central Aegean region during the  
 1598 late Cenozoic. We now review and discuss  
 1599 these conditions.  
 1600

#### 1601 *Conditions at the onset of post-orogenic extension.*

1602 A first inference concerns the mean thickness of  
 1603 the crust at the onset of post-orogenic extension.  
 1604 The present crustal thickness of 25–26 km in the  
 1605 Cyclades suggests an initial thickness of *c.* 43–  
 1606 44 km (see ‘Moho depth’ section and Fig. 7e), in  
 1607 line with the range of *c.* 41–44 km suggested by  
 1608 the width of the Naxos and Paros first-generation  
 1609 MCCs (see ‘Geometry of MCCs’ section and  
 1610 Fig. 7a). These values are consistent with (rough)  
 1611 estimates in the literature (e.g. McKenzie 1978; Le  
 1612 Pichon & Angelier 1979; Gautier *et al.* 1999) and  
 1613 compare well with the current crustal thickness  
 1614 of  $\leq 46$  km in the western Hellenides of mainland  
 1615 Greece (Makris 1975), where extension has played  
 1616 only a minor role.

1617 A second inference concerns the thermal state of  
 1618 the lithosphere at the onset of extension. The  
 1619 numerical experiments suggest an initial thickness  
 1620 of the thermal lithosphere of only *c.* 60 km (cor-  
 1621 responding to an initial Moho temperature of  
 1622 1070 °C at 44 km). Measurements of the present  
 1623 heat flow in the Aegean (Jongsma 1974; Erickson  
 1624 *et al.* 1977; Makris & Stobbe 1984) document the

presence of a hot lithosphere. Seismic surface-wave  
 data are consistent with a lithosphere-asthenosphere  
 boundary at a depth between 40 and 50 km (Endrur  
*et al.* 2008) and, thus, with a high thermal profile of  
 the lithosphere at present. As for the thermal state of  
 the Aegean lithosphere at the onset of post-orogenic  
 extension, it may be deduced from the pressure-  
 temperature path of metamorphic rocks involved  
 in the MCCs.

Figure 10 displays the well-documented cases of  
 Naxos (data from the migmatitic core of the MCC)  
 and Tinos. In the latter case, only the second episode  
 of exhumation is considered (cf. Parra *et al.* 2002) as  
 this is the most likely to reflect post-orogenic exten-  
 sion (see section 3.4). Figure 10 also displays the  
 geotherm associated with an experiment in which  
 the thermal lithosphere is 60 km-thick. The figure  
 shows that, for Naxos, the conditions at the tempera-  
 ture peak coincide with the numerical geotherm. For  
 Tinos, the ‘post-orogenic’ exhumation path starts  
 away from this geotherm and crosses it at conditions  
 equivalent to a pressure of 5 kbar. Geochronological  
 constraints (see sections ‘Post-orogenic versus  
 syn-orogenic extension’ and ‘Timing of exhumation’)  
 suggest that this happens at about the same time  
 (*c.* 21 Ma) as the attainment of peak tempera-  
 tures on Naxos (Fig. 10). Therefore, at this time,  
 Tinos and Naxos plot together along the numerical  
 geotherm. On the one hand, this confirms that a  
 lithosphere only *c.* 60 km-thick is a realistic con-  
 dition at relatively early stages of post-orogenic  
 extension in the Cyclades. On the other hand, the  
 conditions at the onset of the second episode of  
 exhumation on Tinos (550 °C at 9 kbar; Parra  
*et al.* 2002) imply a fairly low geothermal gradient  
 (16.8 °C/km) and plot along a numerical geotherm  
 corresponding to a 100 km-thick lithosphere  
 (dashed line in Fig. 10). Insofar as the entire second-  
 ary exhumation on Tinos reflects post-orogenic  
 extension, this indicates that the earliest stages of  
 this extension occurred while the lithosphere was  
 still thick. The exhumation paths of both Tinos  
 and Naxos are consistent with the view that this  
 lithosphere has been warmed up until the time it  
 attained the conditions enabling the development  
 of interfering MCCs (i.e. a *c.* 60 km-thick litho-  
 sphere), at *c.* 21 Ma. In any case, much of the post-  
 orogenic extensional phase and, within it, the period  
 of development of MCCs occurred while the litho-  
 sphere was thin and hot. This is shown by our  
 numerical results and is also in line with several  
 other numerical studies (Block & Royden 1990;  
 Buck 1991; Tirel *et al.* 2004a, 2008; Rosenbaum  
*et al.* 2005; Wijns *et al.* 2005; Gessner *et al.* 2007).  
 In Figure 10, latest stages of the exhumation paths  
 suggest the existence of geotherms even higher than  
 the one associated with a 60 km-thick lithosphere.  
 This may reflect the ongoing increase of the regional

1625  
1626  
1627  
1628  
1629  
1630  
1631  
1632  
1633  
1634  
1635  
1636  
1637  
1638  
1639  
1640  
1641  
1642  
1643  
1644  
1645  
1646  
1647  
1648  
1649  
1650  
1651  
1652  
1653  
1654  
1655  
1656  
1657  
1658  
1659  
1660  
1661  
1662  
1663  
1664  
1665  
1666  
1667  
1668  
1669  
1670  
1671  
1672  
1673  
1674  
1675  
1676  
1677  
1678  
1679  
1680  
1681  
1682

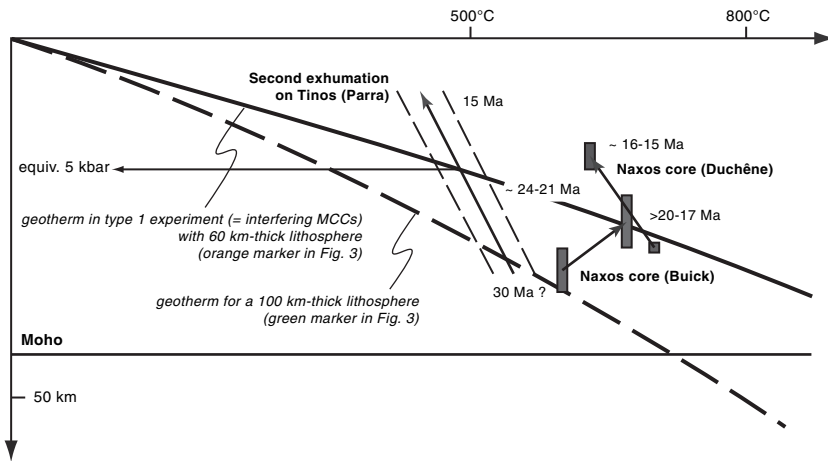


**Fig. 10.** Comparison between the geotherms associated with two numerical experiments and the exhumation path of metamorphic rocks on Tinos (after Parra *et al.* 2002) and Naxos (after Buick & Holland 1989 and Duchêne *et al.* 2006). A factor of 3.64 was used to convert pressures (kbar) into depths (km). Age constraints are discussed in sections ‘Post-orogenic versus syn-orogenic extension’ and ‘Timing of exhumation’.

geothermal gradient or/and the local rise of isotherms during MCC development (see ‘Geometry of MCCs’ section and Gessner *et al.* 2007).

Recently, several studies have shown evidence for a high temperature regime in the shallow mantle and a thin lithosphere (1200 °C at a depth of *c.* 60 km) over widths of 250 to >900 km in several subduction zone back-arc domains unaffected by extensional processes (Currie *et al.* 2004; Hyndman *et al.* 2005; Currie & Hyndman 2006). The authors suggest that heat is rapidly carried upward by vigorous thermal convection in the upper mantle below the overriding plate. This small-scale convection could be promoted by the low viscosities associated with the addition of water, resulting in a reduction of the strength of the base of the lithosphere and its rapid ‘erosion’ (Arcay *et al.* 2005, 2006). The Cyclades area may have been affected by such processes prior to *c.* 21 Ma (i.e. while warming the lithosphere until its thickness was reduced to *c.* 60 km, cf. Fig. 10) provided it was already lying in the back-arc domain of the South Hellenic subduction zone at that time, which is a matter of debate (e.g. Ring & Layer 2003; Jolivet *et al.* 2004; Pe-Piper & Piper 2006).

Alternatively, the pioneering suggestion of Bird (1978) concerning continental mantle delamination as a cause of strong heating of the crust appears attractive. In the Aegean, this process was first suggested by Zeilinger de Boer (1989) and has been explicitly invoked in a number of recent studies (Thomson *et al.* 1999; Jolivet *et al.* 2003; Faccenna *et al.* 2003; Ring & Layer 2003).

Support to this hypothesis is found in a recent review of the late Cenozoic magmatism of the Aegean by Pe-Piper & Piper (2006), as discussed below.

*Boundary velocity during MCC-type extension in the Cyclades.* In the experiments, the range of boundary velocities which successfully led to a sequential development of interfering MCCs lies between 1 and 2.7 cm/a. In addition, the present crustal thickness of 25–26 km in the Cyclades suggests a velocity of *c.* 2.0–2.3 cm/a (see section 4.1.A and Fig. 7f), while the width of the Naxos and Paros first-generation MCCs (see ‘Geometry of MCCs’ section) and the duration of MCC-type extension in the Cyclades (see ‘Timing of exhumation’ section) seem to exclude values lower than *c.* 2 cm/a (Fig. 7b) and *c.* 1.7 cm/a (Fig. 7d), respectively. Hence, the experimental results predict a velocity at the boundary of the stretching domain around 2.0–2.3 cm/a, while lower values seem excluded.

In the case of the Cyclades, this velocity should correspond to the rate at which the South Hellenic subduction retreated during MCC-type extension. In addition, as MCC-type extension in the Cyclades lasted between about 12 and 24 Ma (from 30–23 to 11–6–Ma, see ‘Timing of exhumation’ section), the associated amount of retreat is predicted to lie between about 240 km (for 12 Ma at 2 cm/a) and 550 km (for 24 Ma at 2.3 cm/a).

These values can be compared with various estimates in the literature. For instance, Faccenna *et al.* (2003) have considered 250 km of retreat during the

1683 period from 30 to 5 Ma, hence at a velocity of only  
 1684 1 cm/a. In contrast, a retreat velocity as high as  
 1685 3 cm/a has been proposed by Jolivet *et al.* (1998)  
 1686 on the basis of the southward migration of arc mag-  
 1687 matism since *c.* 32 Ma (Fytikas *et al.* 1984), assum-  
 1688 ing the underlying slab kept a constant dip.  
 1689 However, the graph from which this value is  
 1690 deduced (Jolivet *et al.* 1998, Fig. 21b) actually  
 1691 yields a value of about 2.2 cm/a and considers  
 1692 700 km of migration of arc magmatism, which  
 1693 exceeds by at least 100 km the actual value.  
 1694 Instead, considering about 550 km of migration of  
 1695 magmatism since about 32 Ma (see van Hinsbergen  
 1696 2004 for a recent compilation) would yield a retreat  
 1697 velocity of 1.7 cm/a, in fair agreement with our  
 1698 numerical analysis. However, among the 550 km  
 1699 of migration, as much as 90 km may be considered  
 1700 as balanced, not by extensional strain but by the  
 1701 lateral extrusion of Anatolia during the last few  
 1702 million years (e.g. Gautier *et al.* 1999), which  
 1703 could lower the boundary velocity of the extensional  
 1704 system to 1.4 cm/a. It is also worth noting that the  
 1705 migration of magmatism is not an ideal mean for  
 1706 quantifying retreat, firstly because the assumption  
 1707 of a constant slab dip may not be valid, and secondly  
 1708 because not every magmatic rock may reflect arc  
 1709 magmatism. Pe-Piper & Piper (2006) recently  
 1710 argued that most Cenozoic magmatic rocks of the  
 1711 Aegean bear petrogeochemical characteristics that  
 1712 are not typical of arc processes and suggest instead  
 1713 that they reflect either slab break-off or delamina-  
 1714 tion of the lithospheric mantle. At first sight, this  
 1715 seems to exclude the migration of magmatism as  
 1716 an appropriate tool to document subduction  
 1717 retreat. However, tomography images of the  
 1718 Aegean mantle are clearly more compatible with  
 1719 progressive delamination of a continuous slab  
 1720 (*sensu* Bird 1978) rather than break-off of several  
 1721 slabs (e.g. Faccenna *et al.* 2003; van Hinsbergen  
 1722 *et al.* 2005a). The dynamics of mantle delamination  
 1723 is broadly equivalent to that of a retreating subduc-  
 1724 tion, therefore the migration of delamination-related  
 1725 magmatism may actually be appropriate to quantify  
 1726 retreat (e.g. Zeilinga de Boer 1989).

1727 Another estimate of the amount of retreat may  
 1728 arise from a comparison between the initial and  
 1729 present shape of the Aegean frontal arc. For  
 1730 instance, Gautier *et al.* (1999) suggested a smoothly  
 1731 curved arc at the onset of Aegean extension, which  
 1732 led them to propose about 440 km of retreat (of  
 1733 which 90 km would be balanced by the lateral extru-  
 1734 sion of Anatolia, leaving 350 km to be balanced by  
 1735 extensional strain). The end-member case leading to  
 1736 maximum retreat is probably that of an initially rec-  
 1737 tilinear arc. Using the same arc extremities as in  
 1738 Gautier *et al.* (1999), this case would yield about  
 1739 600 km of retreat, in reasonable agreement with  
 1740 the value suggested by the migration of magmatism.

This would yield about 510 km balanced by extensional strain. If we assume that retreat occurred essentially during MCC-type extension in the Cyclades, then the boundary velocity of the extensional system could have been as high as 2.1 cm/a if extension lasted 24 Ma (starting at *c.* 30 Ma), in good agreement with our numerical analysis, or as high as 4.2 cm/a if extension lasted 12 Ma (starting at *c.* 23 Ma). The latter value is clearly too high and suggests that MCC-type extension in the Cyclades started significantly before 23 Ma or/and that the total amount of retreat has been significantly less than in the above end-member case, or/and that a significant part of the retreat occurred before or/and after MCC-type extension in the Cyclades.

## Conclusions

Our numerical analysis suggests that, for certain conditions, MCCs may interfere and develop in sequence during continental extension. Like common claims in the literature, we find that 'inward' flow of an extremely weak lower crust is required for MCCs to develop, while a sub-Moho mantle of very low strength appears to be another necessary condition for maintaining the Moho flat. As a result of lower crustal inward flow, two conjugate flat-lying shear zones form during the early development of the first MCC, one of which later evolves as a typical detachment. In the experiments with interfering MCCs, the second MCC starts to develop right above one of the previously formed shear zones. This shear zone is dragged upward during dome amplification and, due to renewed inward flow, is reactivated with the same kinematics along one dome limb and with the opposite kinematics along the other dome limb.

The Cyclades archipelago is characterized by three closely spaced chains of MCCs developed largely during Miocene extension. We found that the geometry and kinematic pattern of adjacent MCCs along the Naxos–Ios and the Tinos–Syros transects compare well with the numerical experiments. Available geochronological data for these islands are not detailed enough to document a sequential development of MCCs, nevertheless they remain compatible with this hypothesis. We also compared features of the numerical experiments, such as the final Moho depth, the duration of MCC-type extension, and the width of the domes at the end of the exhumation process, to equivalent features in the Cyclades in order to tentatively constrain the initial and boundary conditions suitable to the Aegean case. This comparison leads us to infer a crustal thickness in the range of 40 to 44 km in the Cyclades at the onset of post-orogenic extension. A thermal lithospheric thickness of only

1741 c. 60 km is also inferred, which might be a condition  
1742 at the onset of extension or may have been obtained  
1743 during early stages of extension while the litho-  
1744 sphere was warmed up. Either a backarc subduction  
1745 setting or a process of mantle delamination may  
1746 account for this situation.

1747 The experiments also suggest a boundary vel-  
1748 ocity of 2.0–2.3 cm/a, which should basically  
1749 reflect the rate at which the South Hellenic subduc-  
1750 tion zone retreated. Considering c. 500 km as an  
1751 upper bound for the amount of retreat balanced by  
1752 Aegean extension, and assuming that this retreat  
1753 mostly occurred during MCC-type extension, in  
1754 the Cyclades, the boundary velocity could have  
1755 been as high as 2.1 cm/a (if MCC-type extension  
1756 lasted 24 Ma, starting at c. 30 Ma and finishing at  
1757 c. 6 Ma): this is in good agreement with the  
1758 numerical analysis.

1760 The post-doctoral grant of C.T. and computational resources  
1761 were funded by ISES (Netherlands Research Centre for In-  
1762 tegrated Solid Earth Science). C.T. thanks E. Burov,  
1763 Y. Podladchikov and A. Poliakov who have co-developed  
1764 the kernel of PARAVOZ. D. J. J. v. H. is funded through  
1765 an NWO-VENI grant. We thank R. Govers, J.-P. Brun and  
1766 E. Burov for discussions at various stages of the project.  
1767 We gratefully acknowledge the editor, M. Edwards, and the  
1768 two reviewers S. Buiter and M. Bröcker for their thoughtful  
1769 reviews that improved our manuscript.

## 1770 References

- 1771  
1772  
1773 ALTHERR, R., KREUZER, H., WENDT, I., LENZ, H.,  
1774 WAGNER, G. A., KELLER, J., HARRE, W. &  
1775 HÖHNDORF, A. 1982. A Late Oligocene/Early  
1776 Miocene high temperature belt in the Attic-Cycladic  
1777 crystalline complex (SE Pelagonian, Greece). *Geo-*  
1778 *logisches Jahrbuch*, **E23**, 97–164.
- 1779 ALTHERR, R., SCHLIESTEDT, M., OKRUSCH, M.,  
1780 SEIDEL, E., KREUZER, H., HARRE, W., LENZ, H.,  
1781 WENDT, I. & WAGNER, G. A. 1979. Geochronology  
1782 of High-Pressure Rocks on Sifnos (Cyclades,  
1783 Greece). *Contributions to Mineralogy and Petrology*,  
1784 **70**, 245–255.
- 1785 ANDRIESSEN, P. A. M. 1991. K-Ar and Rb-Sr age deter-  
1786 minations on micas of impure marbles of Naxos,  
1787 Greece: the influence of metamorphic fluids and lithol-  
1788 ogy on the blocking temperature. *Schweizerische*  
1789 *Mineralogische and Petrographische Mitteilungen*,  
1790 **71**, 89–99.
- 1791 ANDRIESSEN, P. A. M., BOELRIJK, N. A. I. M., HEBEDA,  
1792 E. H., PRIEM, H. N. A., VERDURMEN, E. A. T. &  
1793 VERSCHURE, R. H. 1979. Dating the events of meta-  
1794 morphism and granitic magmatism in the Alpine  
1795 Orogen of Naxos (Cyclades, Greece). *Contributions*  
1796 *to Mineralogy and Petrology*, **69**, 215–225.
- 1797 ANGELIER, J. 1977a. Sur l'évolution tectonique depuis le  
1798 Miocène supérieur d'un arc insulaire méditerranéen:  
l'arc égéen. *Revue de Géographie physique et Géolo-*  
1799 *gie dynamique*, **XIX**, 271–294.
- ANGELIER, J. 1977b. Essai sur la néotectonique et les der-  
niers stades tarditectoniques de l'arc égéen et de l'Égée  
méridionale. *Bulletin de la Société Géologique de*  
*France*, **XIX**, 651–662.
- ANGELIER, J., GLACON, G. & MULLER, C. 1978. Sur la  
présence et la position tectonique du Miocène inférieur  
marin dans l'archipel de Naxos (Cyclades, Grèce).  
*Comptes Rendus de l'Académie des Sciences de*  
*Paris*, **286**, 21–24.
- ARCAÏ, D., TRIC, E. & DOIN, M.-P. 2005. Numerical  
simulations of subduction zones. Effect of slab deshy-  
dration on the mantle wedge dynamics. *Physics of the*  
*Earth and Planetary Interiors*, **149**, 133–153.
- ARCAÏ, D., DOIN, M.-P., TRIC, E., BOUSQUET, R. & DE  
CAPITANI, C. 2006. Overriding plate thinning in sub-  
duction zones: Localized convection induced by slab  
deshydration. *Geochemistry Geophysics Geosystems*,  
**7**, doi:10.1029/2005GC0011061.
- AVIGAD, D. 1993. Tectonic juxtaposition of blueschists  
and greenschists in Sifnos Islands (Aegean Sea)—  
implications for the structure of the Cycladic  
blueschist belt. *Journal of Structural Geology*, **15**,  
1459–1469.
- AVIGAD, D. & GARFUNKEL, Z. 1989. Low angle faults  
above and below a blueschist belt—Tinos Island,  
Cyclades, Greece. *Terra Nova*, **1**, 182–187.
- AVIGAD, D., GARFUNKEL, Z., JOLIVET, L. & AZAÑÓN,  
J. M. 1997. Backarc extension and denudation of Med-  
iterranean eclogites. *Tectonics*, **16**, 924–941.
- AVIGAD, D., BAER, G. & HEIMANN, A. 1998. Block  
rotations and continental extension in the central  
Aegean Sea: palaeomagnetic and structural evidence  
from Tinos and Mykonos (Cyclades, Greece). *Earth*  
*and Planetary Science Letters*, **157**, 23–40.
- AVIGAD, D., ZIV, A. & GARFUNKEL, Z. 2001.  
Ductile and brittle shortening, extension-parallel  
folds and maintenance of crustal thickness in the  
central Aegean (Cyclades, Greece). *Tectonics*, **20**,  
277–287.
- BALDWIN, S. L. & LISTER, G. S. 1998. Thermochronology  
of the South Cyclades Shear Zone, Ios, Greece: Effects  
of ductile shear in the argon partial retention zone.  
*Journal of Geophysical Research*, **103**, 7315–7336.
- BIRD, P. 1978. Initiation of intracontinental subduction in  
the Himalaya. *Journal of Geophysical Research*, **83**,  
4975–4987.
- BLOCK, L. & ROYDEN, L. H. 1990. Core complex geome-  
tries and regional scale flow in the lower crust. *Tec-*  
*tonics*, **9**, 557–567.
- BOND, C. E., BUTLER, R. W. H. & DIXON, J. E. 2007.  
Co-axial horizontal stretching within extending  
orogens: the exhumation of HP rocks on Syros  
(Cyclades) revisited. In: RIES, A. C., BUTLER,  
R. W. H. & GRAHAM, R. H. (eds) *Deformation of*  
*the Continental Crust: The Legacy of Mike Coward*.  
Geological Society, London, Special Publication,  
**272**, 203–222.
- BONNEAU, M. 1982. Evolution géodynamique de l'arc  
égéen depuis le Jurassique supérieur jusqu'au  
Miocène. *Bulletin de la Société Géologique de*  
*France*, **XXIV**, 229–242.
- BOZKURT, E. 2001. Late Alpine evolution of the central  
Menderes Massif, western Turkey. *International*  
*Journal of Earth Sciences*, **89**, 728–744.

- 1799 BRICHAU, S., RING, U., KETCHAM, R. A., CARTER, A.,  
1800 STOCKLI, D. & BRUNEL, M. 2006. Constraining the  
1801 long-term evolution of the slip rate for a major exten-  
1802 sional fault system in the central Aegean, Greece,  
1803 using thermochronology. *Earth and Planetary  
1804 Science Letters*, **241**, 293–306.
- 1805 BRICHAU, S., RING, U., CARTER, A., MONIÉ, P.,  
1806 BOLHAR, R., STOCKLI, D. & BRUNEL, M. 2007.  
1807 Extensional faulting on Tinos Island, Aegean Sea,  
1808 Greece: How many detachments? *Tectonics*, **26**,  
1809 TC4009, doi:10.1029/2006TC001969.
- 1810 BRÖCKER, M. 1990. Blueschist-to-greenschist transition  
1811 in metabasites from Tinos Island (Cyclades, Greece):  
1812 Compositional control or fluid infiltration? *Lithos*, **25**,  
1813 25–39.
- 1814 BRÖCKER, M. & FRANZ, L. 1998. Rb–Sr isotope studies  
1815 on Tinos Island (Cyclades, Greece): additional time  
1816 constraints for metamorphism, extent of infiltration-  
1817 controlled overprinting and deformational activity.  
1818 *Geological Magazine*, **135**, 369–382.
- 1819 BRÖCKER, M. & FRANZ, L. 2000. The contact aureole on  
1820 Tinos (Cyclades, Greece): tourmaline-biotite geother-  
1821 mometry and Rb–Sr geochronology. *Mineralogy and  
1822 Petrology*, **70**, 257–283.
- 1823 BRÖCKER, M. & FRANZ, L. 2005. The base of the Cycladic  
1824 blueschist unit on Tinos Island (Greece) re-visited:  
1825 Field relationships, phengite chemistry and Rb–Sr  
1826 geochronology. *Neues Jahrbuch für Mineralogie,  
1827 Abhandlungen*, **181**, 81–93.
- 1828 BRÖCKER, M. & FRANZ, L. 2006. Dating metamorphism  
1829 and tectonic juxtaposition on Andros Island (Cyclades,  
1830 Greece): results of a Rb–Sr study. *Geological Maga-  
1831 zine*, **143**, 1–12.
- 1832 BRÖCKER, M., BIELING, D., HACKER, B. & GANS, P. B.  
1833 2004. High-Si phengite records the time of greenschist  
1834 facies overprinting: implications for models suggesting  
1835 mega-detachments in the Aegean Sea. *Journal of  
1836 Metamorphic Geology*, **22**, 427–442.
- 1837 BRUN, J.-P., SOKOUTIS, D. & VAN DEN DRIESSCHE, J.  
1838 1994. Analogue modeling of detachment fault  
1839 systems and core complexes. *Geology*, **22**, 319–322.
- 1840 BRUN, J.-P. & VAN DEN DRIESSCHE, J. 1994. Extensional  
1841 gneiss domes and detachment fault systems; structure  
1842 and kinematics. *Bulletin de la Société Géologique de  
1843 France*, **165**, 519–530.
- 1844 BUCK, W. R. 1991. Modes of continental lithospheric  
1845 extension. *Journal of Geophysical Research*, **96**,  
1846 20161–20178.
- 1847 BUICK, I. S. 1991. The late Alpine evolution of an exten-  
1848 sional shear zone, Naxos, Greece. *Journal of the  
1849 Geological Society of London*, **148**, 93–103.
- 1850 BUICK, I. S. & HOLLAND, T. J. B. 1989. The P–T–t path  
1851 associated with crustal extension, Naxos, Cyclades,  
1852 Greece. In: DALY, J. S., CLIFF, R. A. & YARDLEY,  
1853 B. W. D. (eds) *Evolution of Metamorphic Belts*.  
1854 Geological Society, London, Special Publication, **43**,  
1855 365–369.
- 1856 BURG, J. P., VAN DEN DRIESSCHE, J. & BRUN, J.-P.  
1994. Syn to post-thickening extension in the  
Variscan Belt of Western Europe: Modes and  
structural consequences. *Géologie de la France*, **3**,  
33–51.
- BUROV, E. & CLOETINGH, S. 1997. Erosion and rift  
dynamics; new thermomechanical aspects of post-rift  
evolution of extensional basins. *Earth and Planetary  
Science Letters*, **150**, 7–26.
- BUROV, E. B. & GUILLOU-FROTTIER, L. 1999. Thermo-  
mechanical behavior of large ash flow calderas.  
*Journal of Geophysical Research*, **104**, 23081–23109.
- BUROV, E. & POLIAKOV, A. 2001. Erosion and rheology  
controls on synrift and postrift evolution; verifying  
old and new ideas using a fully coupled numerical  
model. *Journal of Geophysical Research*, **106**,  
16461–16481.
- BUROV, E. & POLIAKOV, A. N. B. 2003. Erosional  
forcing on basin dynamics: new aspects of syn- and  
post-rift evolution. In: NIEUWLAND, D. A. (ed.) *New  
Insights into Structural Interpretation and Modelling*.  
Geological Society, London, Special Publication,  
**212**, 209–224.
- BUROV, E. & GUILLOU-FROTTIER, L. 2005. The plume  
head-continental lithosphere interaction using a tectonically  
realistic formulation for the lithosphere. *Geo-  
physical Journal International*, **161**, 469–490.
- BUROV, E. B., JAUPART, C. & GUILLOU-FROTTIER, L.  
2003. Ascent and emplacement of buoyant magma  
bodies in brittle–ductile upper crust. *Journal of Geo-  
physical Research*, **108**, 2177–2189.
- BYERLEE, J. D. 1978. Friction of rocks. *Pure and Applied  
Geophysics*, **116**, 615–626.
- CHÉRY, J. 2001. Core complex mechanics: From the  
Gulf of Corinth to the Snake Range. *Geology*, **29**,  
439–442.
- CONEY, P. J. 1980. Cordilleran metamorphic core com-  
plexes: an overview. In: CRITTENDEN, M. C.,  
CONEY, P. J. & DAVIS, G. H. (eds) *Cordilleran Meta-  
morphic Core Complexes*. Geological Society of  
America Memoir, **153**, 7–31.
- CUNDALL, P. A. 1989. Numerical experiments on localiza-  
tion in frictional materials. *Ingenieur-Archiv*, **59**,  
148–159.
- CURRIE, C. A. & HYNDMAN, R. D. 2006. The thermal  
structure of subduction zone back arcs. *Journal of Geo-  
physical Research*, **111**, B08404, doi:10.1029/  
2005JB004024.
- CURRIE, C. A., WANG, K., HYNDMAN, R. D. & HE, J.  
2004. The thermal effects of steady-state slab-driven  
mantle flow above a subducting plate: the Cascadia  
subduction zone and backarc. *Earth and Planetary  
Science Letters*, **223**, 35–48.
- DAVIS, G. H. 1980. Structural characteristics of meta-  
morphic core complexes, southern Arizona. In:  
CRITTENDEN, M. C., CONEY, P. J. & DAVIS, G. H.  
(eds) *Cordilleran Metamorphic Core Complexes*. Geo-  
logical Society of America Memoir, **153**, 35–77.
- DUBOIS, R. & BIGNOT, G. 1979. Présence d'un 'hard  
ground' nummulitique au sommet de la série crétacée  
d'Almyropotamos (Eubée méridionale, Grèce).  
*Comptes Rendus de l'Académie des Sciences de  
Paris*, **289**, 993–995.
- DUCHÊNE, S., AÏSSA, R. & VANDERHAEGHE, O. 2006.  
Pressure–Temperature–time evolution of metamorphic  
rocks from Naxos (Cyclades, Greece): constraints  
from thermobarometry and Rb/Sr dating. *Geodina-  
mica Acta*, **19**, 301–321.
- ENDRUN, B., MEIER, T., LEBEDEV, S., BOHNHOFF, M.,  
STAVRAKAKIS, G. & HARIJES, H.-P. 2008. *S* velocity  
structure and radial anisotropy in the Aegean region

- 1857 from surface wave dispersion. *Geophysical Journal*
- 1858 **Q4** *International*, in press.
- 1859 ERICKSON, A. J., SIMMONS, G. & RYAN, W. B. F. 1977. Review of heatflow data from the Mediterranean and Aegean Seas. In: BIJU-DUVAL, B. & MONTADERT, L. (eds) *International Symposium on the Structural History of the Mediterranean Basins, Split, Yugoslavia*. Technip, Paris, 263–279.
- 1860
- 1861
- 1862
- 1863
- 1864 FACCENNA, C., JOLIVET, L., PIROMALLO, C. &
- 1865 MORELLI, A. 2003. Subduction and the depth of convection of the Mediterranean mantle. *Journal of Geophysical Research*, **108**(B2), 2099, doi:10.1029/2001JB001690.
- 1866
- 1867
- 1868
- 1869 FORSTER, M. A. & LISTER, G. S. 1999. Detachment
- 1870 faults in the Aegean Core Complex of Ios, Greece. In: RING, U., BRANDON, M. T., LISTER, G. S. &
- 1871 WILLETT, S. D. (eds) *Exhumation Processes: Normal Faulting, Ductile Flow and Erosion*. Geological Society, London, Special Publication, **154**,
- 1872 305–323.
- 1873
- 1874
- 1875 FYTIKAS, M., INNOCENTI, F., MANETTI, P., MAZZUOLI,
- 1876 R., PECCERILLO, A. & VILLARI, L. 1984. Tertiary to
- 1877 Quarternary evolution of volcanism in the Aegean
- 1878 region. In: DIXON, J. E. & ROBERTSON, A. H. F. (eds) *The Geological Evolution of the Eastern Mediterranean*. Geological Society, London, Special Publication, **17**, 687–699.
- 1880
- 1881 GANOR, J., MATTHEWS, A., SCHLIESTEDT, M. &
- 1882 GARFUNKEL, Z. 1996. Oxygen isotopic heterogeneities of metamorphic rocks: an original tectonostratigraphic signature or an imprint of exotic fluids? A case of study of Sifnos and Tinos islands (Greece). *European Journal of Mineralogy*, **8**, 719–732.
- 1883
- 1884
- 1885 GAUTIER, P. 1995. *Géométrie crustale et cinématique de l'extension tardi-orogénique dans le domaine centre-égéen (îles des Cyclades et d'Eubée, Grèce)*. PhD Thesis, University of Rennes 1, France. Mémoires Géosciences Rennes, **61**, 1–417.
- 1887
- 1888
- 1889
- 1890
- 1891 GAUTIER, P. 2000. Comment to “Back-arc extension and
- 1892 denudation of Mediterranean eclogites”. *Tectonics*, **19**,
- 1893 406–409.
- 1894
- 1895 GAUTIER, P. & BRUN, J.-P. 1994a. Ductile crust exhumation and extensional detachments in the central Aegean (Cyclades and Evvia islands). *Geodinamica Acta*, **7**,
- 1896 57–85.
- 1897
- 1898
- 1899
- 1900 GAUTIER, P. & BRUN, J.-P. 1994b. Crustal-scale geometry and kinematics of late-orogenic extension in the central Aegean (Cyclades and Evvia Island). *Tectonophysics*, **238**, 399–424.
- 1901
- 1902
- 1903 GAUTIER, P., BRUN, J.-P. & JOLIVET, L. 1993. Structure and kinematics of Upper Cenozoic extensional detachment on Naxos and Paros (Cyclades Islands, Greece). *Tectonics*, **12**, 1180–1194.
- 1904
- 1905
- 1906
- 1907
- 1908 GAUTIER, P., BRUN, J.-P., MORICEAU, R., SOKOUTIS, D., MARTINOD, J. & JOLIVET, L. 1999. Timing, kinematics and cause of Aegean extension: a scenario based on a comparison with simple analogue experiments. *Tectonophysics*, **315**, 31–72.
- 1909
- 1910 GERBAULT, M., BUROV, E. B., POLIAKOV, A. N. B. &
- 1911 DAGNIÈRES, M. 1999. Do faults trigger folding in the lithosphere? *Geophysical Research Letters*, **26**,
- 1912 271–274.
- 1913
- 1914 GESSNER, K., RING, U., JOHNSON, C., HETZEL, R., PASSCHIER, C. W. & GÜNGÖR, T. 2001. An active bivergent rolling-hinge detachment system: Central Menderes metamorphic core complex in western Turkey. *Geology*, **29**, 611–614.
- GESSNER, K., WIJNS, C. & MORESI, L. 2007. Significance of strain localization in the lower crust for structural evolution and thermal history of metamorphic core complexes. *Tectonics*, **26**, TC2012, doi:10.1029/2004TC001768.
- GRASEMANN, B., EDWARDS, M. A., IGLSEDER, C., PETRAKAKIS, K., SCHNEIDER, D. & Accel Team. 2007. Tertiary SSW directed crustal extension in the Western Cyclades: A new kinematic domain in the Aegean region (Greece). *Geophysical Research Abstracts*, **9**, SRef-ID: 1607-7962/gra/EGU2007-A-06656.
- GOETZE, C. 1978. The mechanisms of creep olivine. *Philosophical Transactions of the Royal Society of London*, **A288**, 99–119.
- GUEYDAN, F., LEROY, Y. M. & JOLIVET, L. 2004. Mechanics of low-angle shear zones at the brittle-ductile transition. *Journal of Geophysical Research*, **109**, B12407, doi:10.1029/2003JB002806.
- HANDY, M. 1989. Deformation regimes and the rheological evolution of fault zones in the lithosphere: the effects of pressure, temperature, grain size, and time. *Tectonophysics*, **163**, 119–152.
- HANSEN, F. D. & CARTER, N. L. 1982. Creep of Selected Crustal Rocks at 1000 MPa. *Eos, Transactions, American Geophysical Union*, **63**, 437.
- HAUSER, E., POTTER, C., HAUGE, T., BURGESS, S., BURTCH, S., MURTSCHLER, J. ET AL. 1987. Crustal structure of eastern Nevada from COCORP deep seismic reflection data. *Geological Society of American Bulletin*, **99**, 833–844.
- HEJL, E., RIEDL, H., SOULAKELLIS, N., VAN DEN HAUTE, P. & WEINGARTNER, H. 2003. Fission-track dating of the south-eastern Bohemian Massif (Waldviertel, Austria); thermochronology and long-term erosion Young Neogene tectonics and relief development on the Aegean islands of Naxos, Paros and Ios (Cyclades, Greece). *Mitteilungen der Österreichischen Geologischen Gesellschaft*, **93**, 105–127.
- HEJL, E., RIEDL, H. & WEINGARTNER, H. 2002. Post-plutonic unroofing and morphogenesis of the Attic-Cycladic complex (Aegea, Greece). *Tectonophysics*, **349**, 37–56.
- HENJES-KUNST, F. & KREUZER, H. 1982. Isotopic dating of pre-alpidic rocks from the island of Ios (Cyclades, Greece). *Contributions to Mineralogy and Petrology*, **80**, 245–253.
- HYNDMAN, R. D., CURRIE, C. A. & MAZZOTTI, S. P. 2005. Subduction zone backarcs, mobile belts, and orogenic heat. *GSA Today*, **15**, 4–10.
- IGLSEDER, C., GRASEMANN, B., PETRAKAKIS, K., EDWARDS, M. A., ZAMOLYI, A., RAMBOUSEK, C., HÖRFARTER, C. ET AL. 2006. Multistage Plutonism and the Serifos Detachment System (Cyclades, Greece). *Geophysical Research Abstracts*, **8**, SRef-ID: 1607-7962/gra/EGU06-A-05118.
- JOLIVET, L. & PATRIAT, M. 1999. Ductile extension and the formation of the Aegean Sea. In: DURAND, B., JOLIVET, L., HORVATH, F. & SÉRANNE, M. (eds) *The Mediterranean Basins: Tertiary Extension within*

- 1915 *the Alpine Orogen*. Geological Society, London, Special Publication, **156**, 427–456.
- 1916 JOLIVET, L., FACCENNA, C., GOFFÉ, B., MATTEI, M.,
- 1917 ROSSETTI, F., BRUNET, C. *ET AL.* 1998. Midcrustal
- 1918 shear zones in postorogenic extension: Example from
- 1919 the northern Tyrrhenian Sea. *Journal of Geophysical*
- 1920 *Research*, **103**, 12123–12160.
- 1921 JOLIVET, L., FACCENNA, C., GOFFÉ, B., BUROV, E. &
- 1922 AGARD, P. 2003. Subduction tectonics and exhumation
- 1923 of high-pressure metamorphic rocks in the Medi-
- 1924 terranean orogens. *American Journal of Science*, **303**,
- 1925 353–409.
- 1926 JOLIVET, L., FAMIN, V., MEHL, C., PARRA, T.,
- 1927 AUBOURG, C., HÉBERT, R. & PHILIPPOT, P. 2004.
- 1928 Strain localization during crustal-scale boudinage
- 1929 to form extensional metamorphic domes in the
- 1930 Aegean Sea. In: WHITNEY, D. L., TEYSSIER, C. &
- 1931 SIDDOWAY, C. S. (eds) *Gneiss Domes in Orogeny*.
- 1932 Geological Society of America Special Paper, **380**,
- 1933 185–210.
- 1934 JONGSMA, D. 1974. Heat flow in the Aegean Sea. *Geophysical*
- 1935 *Journal of the Royal Astronomical Society*, **37**,
- 1936 337–346.
- 1937 KEAY, S., LISTER, G. S. & BUICK, I. 2001. The timing of
- 1938 partial melting, Barrovian metamorphism and granite
- 1939 intrusion in the Naxos metamorphic core complex,
- 1940 Cyclades, Aegean Sea, Greece. *Tectonophysics*, **342**,
- 1941 275–312.
- 1942 KIRBY, S. H. & KRONENBERG, A. K. 1987. Rheology of
- 1943 the Lithosphere: Selected Topics. *Reviews of Geophysics*,
- 1944 **25**, 1219–1244.
- 1945 KIRSCHNER, D. L., COSCA, M. A., MASSON, H. &
- 1946 HUNZIKER, J. C. 1996. Staircase  $^{40}\text{Ar}/^{39}\text{Ar}$  spectra
- 1947 of fine-grained white mica: Timing and duration of
- 1948 deformation and empirical constraints on argon diffusion.
- 1949 *Geology*, **24**, 747–750.
- 1950 KUMERIC, C., RING, U., BRICHAU, S., GLODNY, J. &
- 1951 MONIÉ, P. 2005. The extensional Messaria shear
- 1952 zone and associated brittle detachment faults, Aegean
- 1953 sea, Greece. *Journal of the Geological Society of*
- 1954 *London*, **162**, 701–721.
- 1955 LE PICHON, X. & ANGELIER, J. 1979. The Hellenic arc
- 1956 and trench system: a key to the neotectonic evolution
- 1957 of the eastern Mediterranean area. *Tectonophysics*,
- 1958 **60**, 1–42.
- 1959 LE POURHIET, L., BUROV, E. & MORETTI, I. 2004.
- 1960 Rifting through a stack of inhomogeneous thrusts
- 1961 (the dipping pie concept). *Tectonics*, **23**, TC4005,
- 1962 doi:10.1029/2003TC001584.
- 1963 LI, X., BOCK, G., VAFIDIS, A., KIND, R., HARJES, H.-P.,
- 1964 HANKA, W. *ET AL.* 2003. Receiver function study of
- 1965 the Hellenic subduction zone: imaging crustal
- 1966 thickness variations and the oceanic Moho of the descending
- 1967 African lithosphere. *Geophysical Journal International*,
- 1968 **155**, 733–748.
- 1969 LISTER, G. S., BANGA, G. & FEENSTRA, A. 1984.
- 1970 Metamorphic core complexes of Cordilleran type in
- 1971 the Cyclades, Aegean Sea, Greece. *Geology*, **12**,
- 1972 221–225.
- LOURENS, L. J., HILGEN, F. J., LASKAR, J., SHACKLETON, N. J. & WILSON, D. 2004. The Neogene period. In: GRADSTEIN, F. M., OGG, J. G. & SMITH, A. G. (eds) *A Geologic Time Scale 2004*. Cambridge University Press.
- MAKRIS, J. 1975. Crustal structure of the Aegean Sea and the Hellenides obtained from geophysical surveys. *Journal of Geophysics*, **41**, 441–443.
- MAKRIS, J. 1978. The crust and upper mantle of the Aegean region from deep seismic soundings. *Tectonophysics*, **46**, 269–284.
- MAKRIS, J. & STOBBE, C. 1984. Physical properties and state of the crust and upper mantle of the eastern Mediterranean Sea deduced from geophysical data. *Marine Geology*, **55**, 347–363.
- MAKRIS, J. & VEES, R. 1977. Crustal structure of the Central Aegean Sea and the islands of Evia and Crete, Greece, obtained by refractational seismic experiments. *Journal of Geophysics*, **42**, 329–341.
- MALUSKI, H., BONNEAU, M. & KIENAST, J. R. 1987. Dating the metamorphic events in the Cycladic area:  $^{39}\text{Ar}/^{40}\text{Ar}$  data from metamorphic rocks of the island of Syros (Greece). *Bulletin de la Société Géologique de France*, **3**, 833–842.
- MCCARTHY, J. & THOMPSON, G. A. 1988. Seismic imaging of extended crust with emphasis on the western United States. *Geological Society of America Bulletin*, **100**, 1361–1374.
- MCKENZIE, D. 1978. Active tectonics of the Alpine-Himalayan belt: the Aegean Sea and surrounding regions. *Geophysical Journal of the Royal Astronomical Society*, **55**, 217–254.
- MCKENZIE, D., NIMMO, F., JACKSON, J. A., GANS, P. B. & MILLER, E. L. 2000. Characteristics and consequences of flow in the lower crust. *Journal of Geophysical Research*, **105**, 11029–11046.
- MEHL, C., JOLIVET, L. & LACOMBE, O. 2005. From ductile to brittle: evolution and localization of deformation below a crustal detachment (Tinos, Cyclades, Greece). *Tectonics*, **24**, TC4017, doi:10.1029/2004TC001767.
- MORRIS, A. & ANDERSON, M. 1996. First paleomagnetic results from the Cycladic Massif, Greece, and their implications for Miocene extension directions and tectonic models in the Aegean. *Earth and Planetary Science Letters*, **142**, 397–408.
- MÜLLER, M., GRASEMANN, B., EDWARDS, M. A., VOIT, K., IGLSEDER, C., ZAMOLYI, A. *ET AL.* 2006. Ductile to brittle progressive deformation within crustal-scale shear zones, Western Cyclades, Greece. *Geophysical Research Abstracts*, **8**, SRef-ID: 1607–7962/gr/EGU06-A-06943.
- PARRA, T., VIDAL, O. & JOLIVET, L. 2002. Relation between the intensity of deformation and retrogression in blueschist metapelites of Tinos Island (Greece) evidenced by chlorite-mica local equilibria. *Lithos*, **63**, 41–66.
- PARRISH, R. R., CARR, S. D. & PARKINSON, D. L. 1988. Eocene extensional tectonics and geochronology of the southern Omineca Belt, British Columbia and Washington. *Tectonics*, **7**, 181–212.
- PATZAK, M., OKRUSCH, M. & KREUZER, H. 1994. The Akrotiri unit on the island of Tinos, Cyclades, Greece: Witness to a lost terrane of Late Cretaceous age. *Neues Jahrbuch für Geologie und Paläontologie Abhandlungen*, **194**, 211–252.
- PE-PIPER, G. & PIPER, D. J. W. 2006. Unique features of the Cenozoic igneous rocks of Greece. In: DILEK, Y. & PAVLIDES, S. (eds) *Postcollisional tectonics and*

- 1973 *magmatism in the Mediterranean region and Asia*. Geological Society of America Special Paper, **409**, 259–282.
- 1974 POLIAKOV, A. N. B., PODLADCHIKOV, Y. & TALBOT, C.
- 1975 1993. Initiation of salt diapirs with frictional overburdens: numerical experiments. *Tectonophysics*, **228**, 199–210.
- 1976 RANALLI, G. 1987. *Rheology of the Earth*. Allen and Unwin, Boston.
- 1977
- 1978 REYNOLDS, S. J. & LISTER, G. S. 1990. Folding of mylonitic zones in Cordilleran metamorphic core complexes: evidences from near the mylonitic front. *Geology*, **18**, 216–219.
- 1979
- 1980 RIDLEY, J. 1984. Listric normal faulting and the reconstruction of the synmetamorphic structural pile of the Cyclades. In: DIXON, J. E. & ROBERTSON, A. H. F. (eds) *The Geological Evolution of the Eastern Mediterranean*. Geological Society of London Special Publication, **17**, 755–761.
- 1981
- 1982 RING, U. & LAYER, P. W. 2003. High-pressure metamorphism in the Aegean, eastern Mediterranean: Underplating and exhumation from the Late Cretaceous until the Miocene to Recent above the retreating Hellenic subduction zone. *Tectonics*, **22**(3), 1022, doi:10.1029/2001TC001350.
- 1983
- 1984 RING, U. & REISCHMANN, T. 2002. The weak and superfast Cretan detachment, Greece: exhumation at subduction rates in extruding wedges. *Journal of the Geological Society of London*, **159**, 225–228.
- 1985
- 1986 RING, U., LAYER, P. W. & REISCHMANN, T. 2001. Miocene high-pressure metamorphism in the Cyclades and Crete, Aegean Sea, Greece: Evidence for large-magnitude displacement on the Cretan detachment. *Geology*, **29**, 395–398.
- 1987
- 1988 RING, U., GLODNY, J., WILL, T. & THOMSON, S. N. 2007a. An Oligocene extrusion wedge of blueschist-facies nappes on Evia, Aegean Sea, Greece: implications for the early exhumation of high-pressure rocks. *Journal of the Geological Society of London*, **164**, 637–652.
- 1989
- 1990 RING, U., WILL, T., GLODNY, J., KUMERIC, C., GESSNER, K., THOMSON, S. N. ET AL. 2007b. Early exhumation of high-pressure rocks in extrusion wedges: The Cycladic blueschist unit in the eastern Aegean, Greece and Turkey. *Tectonics*, **26**, TC2001, doi:10.1029/2005TC001872.
- 1991
- 1992 ROESLER, G. 1978. Relics of non-metamorphic sediments on central Aegean islands. In: CLOSS, H., ROEDER, D. & SCHMIDT, K. (eds) *Alps, Apennines, Hellenides*. Inter-Union Commission on Geodynamics Scientific Report, **38**, 480–481.
- 1993
- 1994 ROSENBAUM, G., AVIGAD, D. & SANCHEZ-GOMEZ, M. 2002. Coaxial flattening at deep levels of orogenic belts: evidence from blueschists and eclogites on Syros and Sifnos (Cyclades, Greece). *Journal of Structural Geology*, **24**, 1451–1462.
- 1995
- 1996 ROSENBAUM, G., REGENAUER-LIEB, K. & WEINBERG, R. 2005. Continental extension: From core complexes to rigid block faulting. *Geology*, **33**, 609–612. doi: 10.1130/G21477.1.
- 1997
- 1998 SACHPAZI, M., HIRN, A., NERCESSIAN, A., AVEDIK, F., MC BRIDE, J., LOUCOYANNAKIS, M. ET AL. 1997. A first coincident normal-incidence and wide-angle approach to studying the extending Aegean crust. *Tectonophysics*, **270**, 301–312.
- 1999
- 2000 SÁNCHEZ-GÓMEZ, M., AVIGAD, D. & HEIMANN, A. 2002. Geochronology of clasts in allochthonous Miocene sedimentary sequences on Mykonos and Paros Islands: implications for back-arc extension in the Aegean Sea. *Journal of the Geological Society of London*, **159**, 45–60.
- 2001
- 2002 SCHLIESTEDT, M. & MATTHEWS, A. 1987. Transformation of blueschist to greenschist facies rocks as a consequence of fluid infiltration, Sifnos (Cyclades), Greece. *Contributions to Mineralogy and Petrology*, **97**, 237–250.
- 2003
- 2004 THOMSON, S. N. & RING, U. 2006. Thermochronologic evaluation of post-collision extension in the Anatolide orogen, western Turkey. *Tectonics*, **25**, TC3005, doi:10.1029/2005TC001833.
- 2005
- 2006 THOMSON, S. N., STÖCKHERT, B. & BRIX, M. R. 1999. Miocene high-pressure metamorphic rocks of Crete, Greece: rapid exhumation by buoyant escape. In: RING, U., BRANDON, M. T., LISTER, G. S. & WILLET, S. D. (eds) *Exhumation processes: Normal Faulting, Ductile Flow and Erosion*. Geological Society, London, Special Publication, **154**, 87–107.
- 2007
- 2008 TIREL, C., BRUN, J.-P. & BUROV, E. 2004a. Thermomechanical modeling of extensional gneiss domes. In: WHITNEY, D. L., TEYSSIER, C. & SIDDOWAY, C. S. (eds) *Gneiss Domes in Orogeny*. Geological Society of America Special Paper, **380**, 67–78.
- 2009
- 2010 TIREL, C., GUEYDAN, F., TIBERI, C. & BRUN, J.-P. 2004b. Aegean crustal thickness inferred from gravity inversion. Geodynamical implications. *Earth and Planetary Science Letters*, **228**, 267–280.
- 2011
- 2012 TIREL, C., BRUN, J.-P. & SOKOUTIS, D. 2006. Extension of thickened and hot lithospheres: Inferences from laboratory modeling. *Tectonics*, **25**, TC1005, doi:10.1029/2005TC001804.
- 2013
- 2014 TIREL, C., BRUN, J.-P. & BUROV, E. 2008. Dynamics and structural development of metamorphic core complexes. *Journal of Geophysical Research*, B04403, doi:10.1029/2005JB003694.
- 2015
- 2016 TROTET, F., JOLIVET, L. & VIDAL, O. 2001a. Tectonometamorphic evolution of Syros and Sifnos islands (Cyclades, Greece). *Tectonophysics*, **338**, 179–206.
- 2017
- 2018 TROTET, F., VIDAL, O. & JOLIVET, L. 2001b. Exhumation of Syros and Sifnos metamorphic rocks (Cyclades, Greece). New constraints on the P-T paths. *European Journal of Mineralogy*, **13**, 901–920.
- 2019
- 2020 TURCOTTE, D. L. & SCHUBERT, G. 2002. *Geodynamics*. (2nd ed.) Cambridge University Press, Cambridge.
- 2021
- 2022 URAI, J. L., SCHULING, R. D. & JANSEN, J. B. H. 1990. Alpine deformation on Naxos (Greece). In: KNIPE, R. J. & RUTTER, E. H. (eds) *Deformation Mechanisms, Rheology and Tectonics*. Geological Society, London, Special Publication, **54**, 509–522.
- 2023
- 2024 VAN DER MAAR, P. A. & JANSEN, J. B. H. 1983. The geology of the polymetamorphic complex of Ios, Cyclades, Greece and its significance for the Cycladic Massif. *Geologische Rundschau*, **72**, 283–299.
- 2025
- 2026 VAN HINSBERGEN, D. J. J. 2004. *The evolving anatomy of a collapsing orogen*. PhD Thesis, University Utrecht, The Netherlands. *Geologica Ultraiectina*, **243**, 1–280.
- 2027
- 2028
- 2029
- 2030

- 2031 VAN HINSBERGEN, D. J. J., SNEL, E., GARSTMAN, S. A.,  
 2032 MARUNTEANU, M., LANGEREIS, C. G., WORTEL,  
 2033 M. J. R. & MEULENKAMP, J. E. 2004.  
 2034 Vertical motions in the Aegean volcanic arc:  
 2035 evidence for rapid subsidence preceding volcanic  
 2036 activity on Milos and Aegina. *Marine Geology*, **209**,  
 2037 329–345.
- 2038 VAN HINSBERGEN, D. J. J., HAFKENSCHIED, E.,  
 2039 SPAKMAN, W., MEULENKAMP, J. E. & WORTEL,  
 2040 M. J. R. 2005a. Nappe stacking resulting from subduc-  
 2041 tion of oceanic and continental lithosphere below  
 2042 Greece. *Geology*, **33**, 325–328.
- 2043 VAN HINSBERGEN, D. J. J., LANGEREIS, C. G. &  
 2044 MEULENKAMP, J. E. 2005b. Revision of the timing,  
 2045 magnitude and distribution of Neogene rotations in  
 2046 the western Aegean region. *Tectonophysics*, **396**,  
 2047 1–34.
- 2048 VANDENBERG, L. C. & LISTER, G. S. 1996.  
 2049 Structural analysis of basement tectonites from the  
 2050 Aegean metamorphic core complex of Ios, Cyclades,  
 2051 Greece. *Journal of Structural Geology*, **18**,  
 2052 1437–1454.
- 2053 VANDERHAEGHE, O. 2004. Structural development of the  
 2054 Naxos migmatite dome. In: WHITNEY, D. L., TEYS-  
 2055 SIER, C. & SIDDOWAY, C. S. (eds) *Gneiss Domes in*  
 2056 *Orogeny*. Geological Society of America Special  
 2057 Paper, **380**, 211–227.
- 2058 VANDERHAEGHE, O. & TEYSSIER, C. 2001. Crustal-scale  
 2059 rheological transitions during late-orogenic collapse.  
 2060 *Tectonophysics*, **335**, 211–228.
- 2061 VIGNER, A. 2002. *Images sismiques par réflexions verti-*  
 2062 *cales et grand-angle de la croûte en contexte*  
 2063 *extensif: les Cyclades et le fossé Nord-Egéen*. PhD  
 2064 Thesis, Institut de Physique du Globe de Paris, Univer-  
 2065 sity Paris 7.
- 2066 WALCOTT, C. R. & WHITE, S. H. 1998. Constraints on the  
 2067 kinematics of post-orogenic extension imposed by  
 2068 stretching lineations in the Aegean region. *Tectono-*  
 2069 *physics*, **298**, 155–175.
- 2070 WDOWNSKI, S. & AXEN, G. J. 1992. Isostatic rebound  
 2071 due to tectonic denudation: a viscous flow model of a  
 2072 layered lithosphere. *Tectonics*, **11**, 303–315.
- 2073 WEGMANN, M. I. 2006. *Die Entwicklung des Rb/  
 2074 Sr-Isotopensystems in metamorphen Mikrostrukturen  
 2075 in Abhängigkeit von Temperatur, Druck und Mineralkom-*  
 2076 *position am Beispiel der Hochdruckmetamorphite  
 2077 von Südevia, Griechenland*. Fachbereich Geowis-  
 2078 senschaften, Freie University, Berlin, Germany.
- 2079 WERNICKE, B. 1992. Cenozoic extensional tectonics of the  
 2080 U.S. Cordillera. In: BURCHFIELD, B. C., LIPMAN, P. W.  
 2081 & ZOBACK, M. L. (eds) *The Cordilleran Orogen: Con-*  
 2082 *terminous U.S., The Geology of North America*. Geologi-  
 2083 cal Society of America, **43**, 553–581.
- 2084 WIJBRANS, J. R. & MCDUGALL, I. 1988. Metamorphic  
 2085 evolution of the Attic Cycladic Metamorphic Belt on  
 2086 Naxos (Cyclades, Greece) utilizing  $^{40}\text{Ar}/^{39}\text{Ar}$  age  
 2087 spectrum measurements. *Journal of Metamorphic  
 2088 Geology*, **6**, 571–594.
- WIJBRANS, J. R., SCHLIESTEDT, M. & YORK, D. 1990.  
 Single grain argon laser probe dating of phengites  
 from the blueschist to greenschist transition of Sifnos  
 (Cyclades, Greece). *Contributions to Mineralogy and  
 Petrology*, **104**, 582–593.
- WIJBRANS, J. R., VAN WEES, J. D., STEPHENSON, R. A. &  
 CLOETINGH, S. A. P. L. 1993. Pressure- temperature-  
 time evolution of the high-pressure metamorphic  
 complex of Sifnos, Greece. *Geology*, **21**, 443–446.
- WIJNS, C., WEINBERG, R., GESSNER, K. & MORESI, L.  
 2005. Mode of crustal extension determined by rheologi-  
 cal layering. *Earth and Planetary Science Letters*,  
**236**, 120–134.
- WUST, S. L. 1986. Regional correlation of extension direc-  
 tions in Cordilleran metamorphic core complexes.  
*Geology*, **14**, 828–830.
- ZEILINGA DE BOER, J. 1989. The Greek enigma: is devel-  
 opment of the Aegean orogene dominated by forces  
 related to subduction or obduction? *Marine Geology*,  
**87**, 31–54.